A 2D UNSTEADY INVISCID MODEL
OF SEPARATED FLOW
PAST AN AIRFOIL

By

TODD KIRKLAND PERFITO

Bachelor of Science

Oklahoma State University

Stillwater, Oklahoma

1992

Submitted to the Faculty of the
Graduate College of the
Oklahoma State University
in partial fulfillment of
the requirements for
the Degree of
MASTER OF SCIENCE
December, 1994

A 2D UNSTEADY INVISCID MODEL
OF SEPARATED FLOW
PAST AN AIRFOIL

Thesis Approved:

Andrew L. Arena, Jr.
Thesis Adviser

David G. Lilley

Thomas C. Collins
Dean of the Graduate College

PREFACE

A 2-D discrete vortex model has been developed in order to represent the unsteady aerodynamic forces and moments on airfoil configurations at wide ranges of angle of attack (from 0 - 85 degrees). The assumptions are that of an inviscid, incompressible flowfield and for the chordwise steady state location of the separation points to be input as known from experiments or flow visualization. Preliminary results indicate that assuming a separation point determined from experimental data is in good agreement with post stall aerodynamic data. The model qualitatively captures the separated flowfield characteristics observed from experiment. The model has also been applied to a tandem airfoil configuration in order to investigate the interaction between the separated wake and a longitudinal control surface. In addition, the model has been used to simulate oscillatory motion for attached flow and ramp motion for separated flow.

TABLE OF CONTENTS

LIST OF FIGURES

NOMENCLATURE

a .... normal component influence coefficient

b .... tangential component influence coefficient

c .... chord length

C_l .... sectional lift coefficient

C_m .... sectional moment coefficient

C_{lt} .... sectional lift coefficient (wing&tail)

C_{mt} .... sectional moment coefficient (wing&tail)

C_p .... pressure coefficient

dl .... panel length

d .... tail distance from main airfoil

h .... tail height above body fixed x-axis

h/c .... nondimensional plunge height

i .... tail incidence angle (+ ccw)

t .... time

U .... freestream velocity

V .... total velocity at a point

V_∞ .... freestream velocity

x .... body fixed chordwise coordinate

z .... body fixed normal coordinate

α .... angle of attack

α_{nd} .... nondimensional rate of chage of angle of attack

Φ .... velocity potential

Φ_∞ .... freestream velocity potential

γ .... vortex strength

γ_t .... vortex strength at time t

$\gamma_{t-\Delta t}$ .... vortex strength at previous time step

γ_s .... nascent vortex strength

Γ .... circulation

θ .... panel angle relative to body fixed coord.

CHAPTER I

INTRODUCTION

1.1 Problem Statement

The formation of unsteady separated flow fields is a problem encountered in a variety of applications. These complex flow fields are characterized by large scale vortex formations. They are seen, for example, in rotor craft and turbomachinery, maneuvering underwater vehicles and form on turbines. The understanding of these complex physical interactions that occur between the different regions that make up the separated flowfield is a major concern for aerodynamicists. Indeed, unsteady aerodynamics may be the ultimate manner in which to achieve highly maneuverable flight vehicles, as well as extremely efficient turbomachinery. However, before schemes can be developed or employed to utilize the energy within unsteady flows, complete understanding, with the ability to predict and control the processes, of these unsteady complex flows must be attained. The most common method of computing these complex flow fields has been to employ dense finite difference schemes to solve the momentum equation of the Navier-Stokes equations. However, this technique imposes large demands on today's computing power. A more fundamental scheme to aid in the understanding of separated flows must be used to speed and simplify the process. The development and utilization of vortex methods has greatly enhanced the capabilities of the aerodynamicist to investigate more complex flows in a shorter amount of time.

1

1.2 Background Literature Review

As in any research endeavor a thorough literature search was performed to determine what work has been done using unsteady vortex methods. Several different schemes have been utilized to model unsteady flow. These include analytical approaches, to investigate the usefulness of classical small disturbance approximations and complex variable exact solutions, as well as vortex methods and panel methods, to simulate numerically the unsteady flow. Unsteady vortex methods have been used by numerous authors, and a list of the application of these methods is included in Clements & Maull.[1] Sarpkaya[2] gives a comprehensive and extensive review of computational methods with vortices from theoretical foundations to practical applications. The first use of classic analytical potential flow theory for thin plates executing small amplitude, simple harmonic motion has been presented by Karman & Sears[3] and Theodorsen.[4] Theordorsen was the first to publish the analytic solution for simple harmonic motion. His solution gives an illuminating division of the circulatory and noncirculatory portions of the potential flow. The theory of transient motions of flat plates has been developed by Wagner[5] and Küssner.[6] The effects of thickness of airfoils in small amplitude, simple harmonic motion has been studied by Küssner,[7] Van De Vooren,[8] and Hewson-Brown,[9] who use a circle-airfoil conformal mapping technique.

In addition to the analytic work mentioned, early work by Basu & Hancock[9] use a numerical approach for the calculation of the pressure distribution, forces, and moments on a two-dimensional airfoil undergoing arbitrary unsteady motion in an inviscid incompressible flow. The study is limited to attached flows separating only at the trailing edge. Its application is directed towards an airfoil having a sudden change in incidence, oscillating at high frequency, or passing through a sharp edge gust. The model is based on the steady method used by Hess & Smith[11] that utilizes a distribution of source-vortex panels on the airfoil. However Basu & Hancock adjusted this technique by adding a

2

vortex wake panel at the trailing edge. This method is applied step-by-step in time, starting from a given initial airfoil position and orientation and proceeding step-by-step along the airfoil path. A time dependency is introduced at each step in time by using the total change in circulation generated by the airfoil to be shed into the wake, via the wake panel, so that the total circulation generated by the airfoil sums to zero, i.e. the Kelvin condition. The uniqueness of the solution is invoked by specifying that the pressures at the closest collacation points to the trailing edge be equal, which can also be considered to enforce zero loading across the shed vorticity, i.e. the shear layer. Giesing[12] shows that the solution from the condition of $\Delta p=0$ is analytically equivalent to that of $\Delta V=0$. As a result however, the condition of equal pressures at the trailing edge adds a nonlinearity to the system of equations. This nonlinearity stems from the use of the unsteady Bernoulli equation and therefore requires an iterative procedure for the solution. The unsteady inviscid model based from the Hess & Smith approach is widely accepted as a practical procedure for solving attached unsteady flowfield problems.

If we follow the assumption that for high Reynolds number flows the viscous effects are confined within thin shear layers, then this assumption might also be extended to a separated flow analysis where the pressure distribution and its integrated effects are desired. Accordingly, there has been some success in the representation of separated flows on two-dimensional airfoils using vortex models. The principles of the discrete vortex method for modelling airfoils with boundary layer separation were summarized by Sears.[13] The vortex shedding behind a flat plate was analyzed by Sarpkaya,[14] who calculated the strength of the emanating vorticity layers by the shear velocity method. A different method for the calculation of the shed vorticity strength was applied by Kiya & Arie.[15] They introduced the nascent vortices at a fixed location, while its strength was calculated by the Kutta condition. The above cited literature shows the efforts conducted to reduce the viscous problem into a simpler potential model. However, there are codes like that developed by Mehta[16] which are based on the solution of the Navier-Stokes

equations. Again, the major drawbacks of these codes are the large computer times and memory required relative to the time and memory required for the much simpler discrete vortex methods.

It is shown in Sears[13] that the condition that determines circulation about an airfoil with boundary layers is "identical with the usual inviscid flow condition based on the conservation of total circulation and the Kutta condition, in both steady and unsteady flow."[6] Interesting relationships between the viscous and inviscid models are discussed, namely, between boundary layer vorticity and bound vortex strength, and viscous wake vorticity and free vortex strength in both steady and unsteady flow. The unsteady aerodynamics of airfoils with rounded trailing edges are considered, and it is concluded that a dual model is needed, involving a boundary layer calculation over a smooth body to determine circulation, and a vortex sheet model to determine the perturbed potential flowfield, as well as forces and moments on the airfoil. It is disputed that the bound vortex sheet on the airfoil does represent the airfoil plus its boundary layers, and that the shed vortex wake behind the airfoil does represent simply the vortical viscous wake that forms at the termination of the boundary layers. "This serves to remind us that the inviscid fluid model must represent the limiting case of vanishingly small viscosity and not the flow of a truly inviscid fluid."[13]

Previous studies by Katz[17] analyzed a post stall regime. Katz simulated the flowfield with a two dimensional vortex lattice method using a thin cambered airfoil modeled with discrete vortices along its camberline as well as the shed wakes being modeled with discrete vortices. The main focus being the validation of the model with experiments and also made observations into the periodic wake shedding pattern. The shed vorticity was given an initial strength equal to the difference in average velocities evaluated above and below the shear layer near the separation point. The validity of which was demonstrated experimentally by Fage & Johansen.[18] The model was considered to be accurate considering that it used thin airfoil assumptions as well as the

introduction of circulation reduction and amplification factors to better approximate experimental observations. However, the results were accurate and do add validity to the inviscid assumption.

Vortex methods have also been used successfully by Arena & Nelson[19] who modeled the complex phenomenon of wing rock with an inviscid unsteady aerodynamic model coupled with the roll degree of freedom. The model used was based on an unsteady complex potential formulation in the context of a slender wing theory. The slender wing formulation used a 2-D conical approach with two leading edge potential vortices separating at the leading edges of a delta wing. This simulated the spiral shear layers that emanate from a delta wing in stall below angles of attack where vortex breakdown is present. The most fundamental assumption was that all the vorticity in the system was confined to the cores of the two leading edge vortices. In fact, the computational model did reveal the primary mechanisms involved in wing rock.

A more complex use of vortex methods with separated flow was accomplished by Huyer, Grant, & Uhlman.[20] They utilize constant vorticity elements to model the vorticity production, accumulation, and transport mechanisms for unsteady separated flows past stationary and moving surfaces. Vorticity is produced in such a manner as to satisfy the no-slip and no-flux boundary conditions at the airfoil surface. Thus this particular study does not use an inviscid flow assumption. It uses the inverse of the input Reynolds number to set the value of the nondimensional kinematic viscosity, the freestream and the airfoil chord length are equal to unity, to be used in the vorticity equation. In addition, the elements are of constant vorticity and finite area and are allowed to deform. The strengths of the vortex elements originating on the body surface are determined by requiring that the velocity induced by the vortex element be equal and opposite to the velocity at the surface. The temporal evolution of the vorticity field is then computed using the Biot-Savart law. The vortex elements are then transported by the local velocity field. Unique features for this research include splitting and

amalgamation of the vortex elements as the elements deform, as well as a random walk technique, first used by Chorin,[21] to simulate the effects of diffusion. This method is then used to analyze separated flow past a cylinder and a NACA 0015 airfoil undergoing a single pitch up motion from 0 to 60 degrees angle of attack. Comparisons with previous experimental data show good quantitative similarities. The complexities of this particular model can be considered the extent to which vortex methods might be applied to simulate viscosity.

1.3 Summary

The prediction of an airfoil's dynamic loading and resulting motion is directly related to the validity of the aerodynamic solution. Several methods are available to help predict an airfoil's loading and resulting motion from simple two dimensional linear methods to full scale three dimensional Navier Stokes codes. Aerodynamic calculations with Navier Stokes codes, while accurate, are extremely time intensive making the technique presently inadequate for advanced flight dynamic studies in a post stall regime, where the amount of required calculations to satisfactorily describe the flow field solution would severely limit the speed capabilities of the computer. A variety of simplifications can be used to increase the speed of the solution depending on the accuracy required. If the accuracy of the solution can be maintained and the speed of the solution increased, then more scenarios can be considered in a given amount of time, thereby giving more time to analyze further those scenarios that show prevalence.

One basic idea is to look at the two dimensional flowfield where most of the mechanics are present but the three dimensional interactions have been dropped. Another simplification is defining the flow to be inviscid, i.e. a potential flow. It can be maintained for gases, such as air moving at a high Reynolds number, that viscosity effects are mainly confined to the boundary layer and separated shear layers. If this assumption

can be used and the solution can be validated with experimental results, then this technique can be a useful tool in analyzing complex two-dimensional flows and possibly extrapolated into a three-dimensional regime. So, rather than attempting to define, control, and monitor the complete discretized flowfield region, as a Navier Stokes analysis would, only those parts that influence the flow are kept. This scheme can be considered most useful for determining integrated effects where the need to capture more detailed effects is not necessary.

1.4 Objectives of the Present Investigation

It is of some interest to know to what extent the potential flow theory models may be applied to separated flows in order to significantly reduce computation time. Is it possible to represent the large chaotic wake behind an airfoil at high angles of attack with an inviscid discrete vortex wake model rather than using Navier-Stokes codes to model an entire discretized control area? Does the solution compare to experimental observations for a given set of circumstances? Can the moving separated shear layer be modeled accurately to give a true representation of this complex flow? This research will attempt to explore and address these questions. More specifically, in order to address these questions, the following unsteady flow investigations have been performed:

i.)   Attached flow cases are analyzed and compared with theoretical and analytical solutions to validate the unsteady model for both static and dynamic conditions.

ii.)   Separated flow examples, both static and dynamic, are then carried out to determine the value of an extension of the inviscid assumption to separated flows.

Accordingly, the objective of the current study is to develop a simplified 2-D unsteady model of complex separated flow fields to ascertain the applicability of the technique to separated flows by comparing results obtained by others with those obtained here.

CHAPTER II.

COMPUTATIONAL MODEL

2.1 Governing Equation

Real fluids are all viscous. Chow[22] states that viscosity is caused by "the redistribution of excessive momenta among neighboring fluid molecules through the action of intermolecular collisions." Thus a viscous force is exerted on the surface of a fluid element where a local velocity gradient is present. It may be either a shearing force tangent to the surface, such as one found in a boundary layer, or a normal force that exists, for example, within a shock wave. The importance of the viscous force in comparison to the inertial force is represented by the Reynolds number, which is the ratio of a characteristic inertial force to a characteristic viscous force. For flows such as air and water, the Reynolds number is usually quite high, and the inertial forces will dominate over the much smaller viscous forces. This assumption taken to the limiting case is known as an inviscid flow.

Inviscid flow analysis is justified for high Reynolds number where the effect of viscosity is confined to thin boundary layers. It is assumed in inviscid theory that these layers contain all the vorticity of the system. It is also assumed that, although the shed wake is thick for separated flow, the modelled separated shear layer is thin and continuous. This assumption is an extension of Prandtl's[23] postulation to allow for separation in an inviscid flow. Outside these shear layers an irrotational (potential) flowfield exists. This irrotationality condition states that the vorticity vanishes, i.e.

8

$\nabla \times \mathbf{q} = 0$, where q is the velocity vector (**u**,**w**). The irrotationality is automatically satisfied if a velocity potential is introduced such that $\mathbf{q} = \nabla\Phi$. Therefore, if the fluid is assumed incompressible, the velocity field must also satisfy the continuity equation, $\nabla \cdot \mathbf{q} = 0$. So upon substitution this yields Laplace's equation:

$$\nabla^2\Phi = 0 \qquad\qquad (1)$$

which is a second order linear homogeneous partial differential equation (PDE).

2.2 Choice of Singularity

Since the linear combination of elementary solutions to a homogeneous PDE also has a solution, the principle of superposition can be used to model an arbitrary flowfield. The elementary solutions to Laplace's equation, such as sources and vortices, can be superimposed to form a particular streamline boundary or potential flux for some given flowfield. These elementary solutions can be of a discrete nature or of some distributed strength and their combinations will still result in, if given a condition of uniqueness, a singular solution to Laplace's equation. Superposition can then serve as a method for which an array of linearly independent elementary solutions, distributed with unknown strengths, in a manner that will satisfy each boundary condition, can be solved in order to model an inviscid flowfield. This use of Laplace's equation and superposition is known as a paneling method.

Figure 1 shows the orientation of the individual panels of an airfoil with ten source-vortex panels. Also shown are the angles and lengths, $(r_1,r_2,\Theta_1,\Theta_2)$, used in the equations that follow. The dashed line in Figure 1 represents the vortex strength, (γ), which are equal for all panels.

9
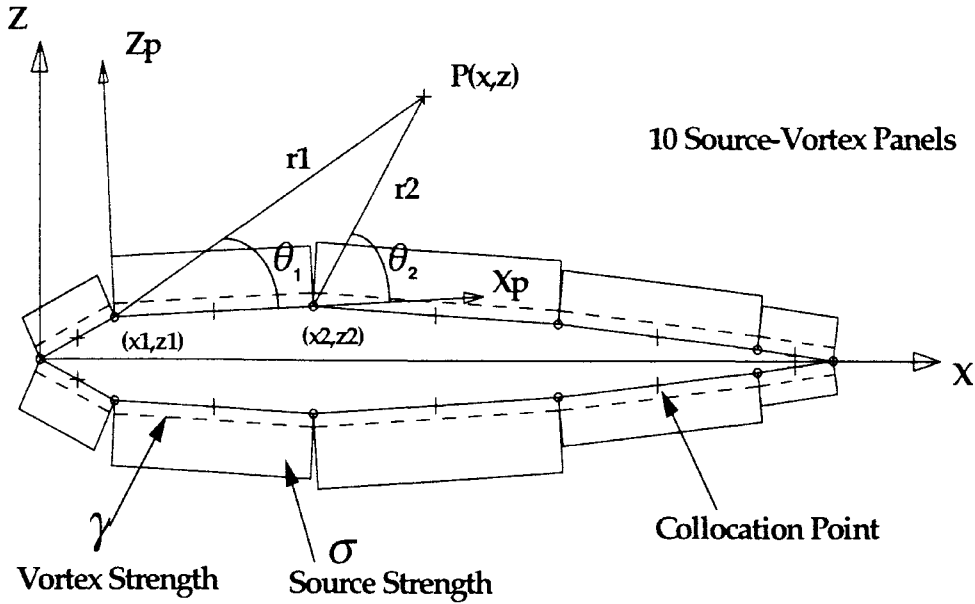
Figure 1. Airfoil with panel layout.

For the present study, a constant strength source-vortex paneling method was used to model an airfoil. A constant strength source-vortex panel is the combination of a uniformly distributed (constant) strength source panel with that of a constant strength vortex panel. Figure 1 shows the basic geometry of the system. The airfoil shown is a NACA0012 approximated with 10 constant strength source-vortex panels, usually 80 were used. The global panel coordinate system is shown at the leading edge of the airfoil as well as a local panel coordinate panel system on the upper surface of the airfoil. The panels are numbered consecutively starting from the lower trailing edge and then moving clockwise around the airfoil. The local panel coordinate system is situated such that the local x-axis is always pointing to the next higher panel number. The induced cartesian velocities on some arbitrary point p for a constant strength source panel are:

$$u_{sp_p} = \frac{\sigma_j}{2\pi} ln \frac{r_1}{r_2}$$

$$w_{sp_p} = \frac{\gamma_j}{2\pi}\left(\Theta_2 - \Theta_1\right)$$

(2)

The induced cartesian velocities for a constant strength vortex panel are given as:

$$u_{vp_p} = \frac{\gamma_j}{2\pi}\left(\Theta_2 - \Theta_1\right)$$

$$w_{vp_p} = \frac{\sigma_j}{2\pi} \ln \frac{r_2}{r_1}$$

(3)

These equations represent those velocities that are induced by some constant strength panel j on some arbitrary point p.

2.3 Boundary Conditions

The distribution and superposition of the singularities can serve to provide a solid boundary for which flow is held outside this boundary. This condition is enforced by defining the flow normal to each panel collocation point, see Figure 1, to be zero for a non-moving airfoil. This is known as the Neumann boundary condition and can be shown as:

$$\nabla\left(\Phi + \Phi_\infty\right) \cdot n = 0$$

(4)

where Φ is the perturbation (disturbance) potential and Φ_∞ is the freestream potential:

$$\Phi_\infty = U_\infty x + W_\infty z$$

(5)

Also, the perturbation velocity induced by the airfoil motion must decay far from the airfoil,

$$\nabla \Phi = 0 \qquad \text{as } r \rightarrow \infty \qquad\qquad (6)$$

which is identically satisfied from equations 2 & 3. This formulation does not yet uniquely describe a solution since a large number of singularity distributions will satisfy any given set of boundary conditions. Furthermore, the boundary conditions given so far are for steady flow.

2.4 Influence Coefficients

With the choice of the singularity distribution and the definition of the steady boundary conditions, influence coefficients can be determined for each singularity. An influence coefficient defines the velocity influence induced from a given singularity with a unit strength on all other singularities knowing their position relative to the other.

Specifically, the gradient of the total potential is defined as the total velocity vector, i.e. $\nabla \Phi = \hat{q}$, where

$$\hat{q} = \left(u + U_\infty\right)\hat{i} + \left(w + W_\infty\right)\hat{k} \qquad\qquad (7)$$

and (u,w) is the perturbation velocity. So that

$$\nabla \Phi \cdot \hat{n} \equiv \hat{q} \cdot \hat{n} \qquad\qquad (8)$$

with

$$\hat{n} = -\sin\beta\,\hat{i} + \cos\beta\,\hat{k} \tag{9}$$

and β is the panel angle with respect to the airfoil's global x-z coordinate system

$$\beta = \operatorname{atan}\big[(z_2 - z_1)/(x_2 - x_1)\big] \tag{10}$$

The perturbation velocity, (u,w), of equation (7) can be represented by a combination of influence coefficients while the freestream and previously shed wake contributions are known and can be transferred to the right hand side (RHS) of the system of equations shown in the next section. Consequently, the influence coefficients can be defined as

$$a_{i,j} = (u,w)_{i,j} \cdot \hat{n}_i \tag{11}$$

where the velocities induced, (u,w), are at panel i from panel j. This makes the normal influence coefficients, $a_{i,j}$, only a function of geometry. So then,

$$
\begin{aligned}
\hat{q}_1 \cdot \hat{n} &= \big(a_{11}\sigma_1 + a_{12}\sigma_2 + \ldots + a_{1n}\sigma_n\big)_{sp} \\
&\quad + \big(a_{11}\Gamma_1 + a_{12}\Gamma_2 + \ldots + a_{1n}\Gamma_n\big)_{vp}
\end{aligned}
\tag{12}
$$

where σ and Γ are unknowns. At this point we choose to hold $\Gamma_1 = \Gamma_2 = \Gamma_n = \Gamma_{\text{wing}}$ to simplify the solution process by keeping the number of equations required to solve at a minimum. So applying the zero normal flow boundary condition to panel 1 yields:

$$\left(a_{11}\sigma_1 + a_{12}\sigma_2 + \ldots + a_{1n}\sigma_n\right)_{sp} \cdot n_1 +$$
$$\left(a_{11} + a_{12} + \ldots + a_{1n}\right)_{vp} \Gamma_{airfoil} \cdot n_1 + \left(U_\infty, W_\infty\right) \cdot n_1 = 0 \tag{13}$$

This satisfies the solid body boundary condition and gives N equations for N+1 unknowns and still does not include an unsteady term or a condition for uniqueness.

Equally useful are the tangential influence coefficients to be used in later boundary conditions. They are defined as

$$b_{i,j} = (u,w)_{i,j} \cdot \hat{t}_i \tag{14}$$

with

$$\hat{t} = \cos\beta\,\hat{i} + \sin\beta\,\hat{k} \tag{15}$$

2.5 Kutta Condition

For all that the previous sections described, an unsteadiness and a constraint for uniqueness has yet to be introduced. This section and the following sections introduce time dependencies and their subsequent effects as well as a method for specifying uniqueness.

First of all, circulation is needed to generate lift. The solution to equation 13 can be made to be unique by specifying any arbitrary value for the circulation Γ. If the circulation is modelled by a vortex distribution, then integration of the vorticity distribution around the airfoil surface yields the total circulation for the airfoil. However, for the solution to be viable, certain physical constraints must be met to provide the correct value of circulation in the solution. Since the trailing edge angle is finite the

normal component of the velocity, from both sides of the airfoil, must vanish. For a continuous velocity, this is possible only if this is a stagnation point. Therefore, it is useful to assume that the pressure difference there is also zero. Thus for the steady case, this can also be viewed as requiring the vorticity to be zero at the trailing edge. These last three statements can all be considered as a statement of the Kutta condition.

The Kutta condition provides the boundary condition that yields a unique solution to the flowfield. Giesing[24] showed, for steady flow, that the Kutta condition is for the velocities on the upper and lower surfaces of the airfoil's trailing edge to be equal in magnitude but opposite in tangential direction to force the velocity at the trailing edge to be zero. Katz & Plotkin[25] show that this condition can also be used for unsteady flow when the reduced shedding frequency is relatively high, $\omega c/2U_\infty = 8.5$. Their steady Kutta condition yielded very good results for a wide range of unsteady flows. This particular scheme of setting the trailing edge velocities to be zero is the Kutta condition that will be used here. However, they do recommend some caution in this Kutta's use when large angles of attack or large trailing edge displacements are encountered.

There are alternatives to the chosen Kutta. As mentioned earlier, Basu & Hancock[10] use a condition of equal pressures at the trailing edge rather than velocities being equal there. Again, this adds a nonlinearity to the system of equations and an iterative scheme must be used. Specifically, this would entail solving the linear portion of the equations, resulting in some solution in terms of a circulation, this circulation is then determined from the quadratic equation obtained from the pressure equation set up for the trailing edge, namely the difference in the squares of the two velocities at the upper and lower surface of the trailing edge being equal to the rate of change in circulation on trailing edge wake element. This scheme is another effective use of the Kutta condition for specifying uniqueness, however due to the nonlinearity it was not chosen.

2.6 Kelvin Condition

Time dependency, which has not yet been defined, is introduced through boundary conditions since the Laplace equation, the governing equation for inviscid flow, does not directly include time dependent terms. Time dependency is given by the circulation condition, Kelvin's theorem, which states that the time rate of change of circulation around a closed curve is zero, such that:

$$\frac{D\Gamma}{Dt} = \frac{\Gamma_{airfoil} + \Sigma\Gamma_{wake}}{\Delta t} = 0 \tag{16}$$

i.e. angular momentum conservation. Therefore,

$$\Gamma_{airfoil} + \Sigma\Gamma_{wake} = 0 \tag{17}$$

By this it is meant that the circulation generated by the airfoil must also be shed into the wake, so that the total circulation in the flowfield at any given time sums to zero. This boundary condition actually gives the system of equations the time dependency desired for an unsteady solution.

Therefore, the circulation generated by the airfoil is shed into the wake as a point vortex which represents the transition of the bound vorticity, i.e. the boundary layer, into the force free shear layer, see Figure 2. The shed vortices are then convected downstream by calculating the induced velocity on each vortex from the freestream, the airfoil panels, and the other previously shed vortices and multiplying this velocity by the nondimensional time step.
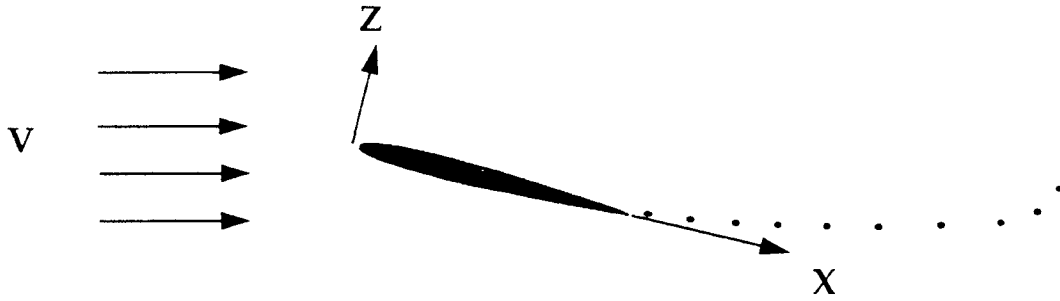
Figure 2. Flowfield model with representative separated vortices at trailing edge.

A major problem with discrete vortex models is the induced velocity calculation. A potential vortex is singular at its center, and the induced velocity near its center is unrealistically large. This can cause difficulties in the pressure calculation when a vortex is near the body surface and in the vortex trajectory calculation when two or more vortices are in close proximity. The typical solution is the use of a vortex core model to remove the singularity at the origin.

Numerous core models have been proposed and used successfully by various investigators. These range from a simple cutoff distance, inside which the vortex induced velocity is set to zero, to a solid body rotation model that enforces a linear velocity distribution from zero at the vortex center to the potential value at a specified radius. The core model used here, obtained from Mendenhall et al.,[26] is given by:

$$v_\Theta(r, r_c) = (\Gamma/2\pi \ r)(1 - \exp(-1.256 r / r_c)^2)$$

(18)

where r is the distance to an arbitrary point and r_c is the core size, being the nondimensional time step in this case. This confines the vorticity to the core region while maintaining a potential flow outside, as well as keeping the shape of the wake realistic. This core model may also be seen in Figure 3. Also no vortex cutoff, dissipation, or

17

amalgamation techniques were used to improve speed performance since simplicity is a main concern.
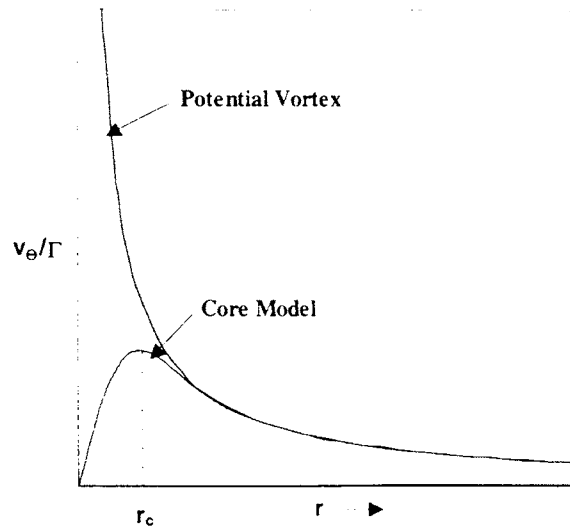
Figure 3. Vortex induced velocity model.[26]

2.7 Separation Modeling

The points of separation are chosen to be the trailing edge and some point along the top of the airfoil given by experimental observations. As a result, the tangential velocity at the point of secondary separation on top of the airfoil is set to zero and the trailing edge tangential velocities at the closest neighboring collocation points are to sum to zero. The use of tangential velocities for the trailing edge separation point rather than total velocities is preferred in this context to keep nonlinearities from entering the system of equations, thereby simplifying the solution method to one of a linear nature.
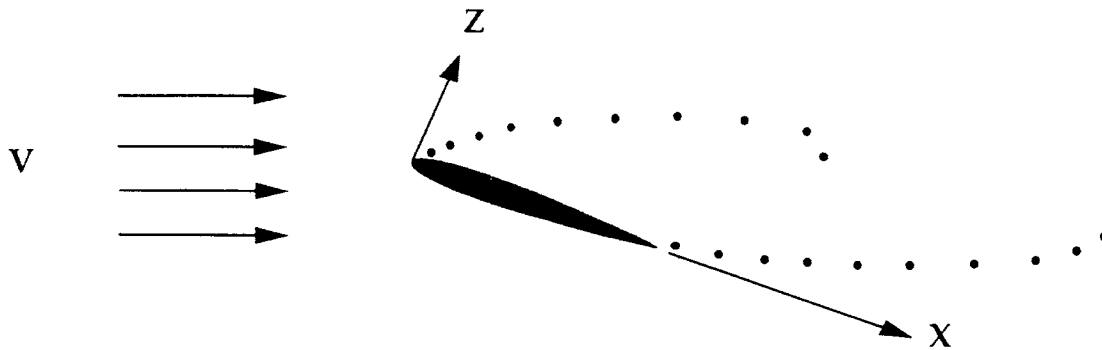
Figure 4. Flowfield model with representative separated vortices at trailing edge and leading edge.

To obtain a continuous and finite velocity distribution the points of separation are considered stagnation points. It has already been shown that the trailing edge stagnation point is set by enforcing equal tangential velocities at the closest neighboring collocation points through the Kutta condition. Furthermore, the upper separation point is enforced by setting a boundary condition such that the tangential velocity at the point of separation is equal to zero. The enforcement of this separation point is also accomplished through the use of the Kutta condition. The new upper separation point also requires a modification to the Kelvin condition to account for the added vorticity shed there. However, in terms of equation 17, the added vorticity to the wake is accounted for by the summation.

The position of the upper separation point is allowed to move as a function of the airfoil pitch rate and of time using a state-space representation. The rationale of this approach is to simplify the solution process. If a boundary layer routine was incorporated into the solution scheme, the time required for solution would significantly increase. It is known from many studies of dynamic stall, such as Jumper,[27] that in the presence of a positive α the airfoil flow separation is delayed to higher angles of attack compared to the steady separation point location. Goman[28] showed successfully that the nonlinear

behavior of the separation point's unsteady motion can be described simply by the first order differential equation

$$\tau_1 \frac{dx}{dt} + x = x_0\left(\alpha - \tau_2\dot{\alpha}\right)$$ (19)

where τ_1 and τ_2 are time constants which outline the relaxation of the separation process and delay of its inception and x_0 is the steady state separation point location as a function of α. $x_0(\alpha-\tau_2\dot{\alpha})$ is understood as the steady state separation location as a function of $(\alpha-\tau_2\dot{\alpha})$. The steady state separation point location as a function of angle of attack is approximated from experimental data obtained from Katz.[17] The motivation behind the use of previous experimental data for the location of the static separation point location as a function of angle of attack is that a curve fit may be utilized so that the state-space representation of the separation point transition may be performed. The state-space transition model is referenced to be applicable for relatively small rates of variation of angle of attack, Goman sites $\dot{\alpha} \le 0.02 V_\infty/c$. However, this applicability is in reference to the closed mathematical model that Goman developed where C_l and C_m were given as expressions obtained from the assumptions that the separated flow could be modelled by "Kirchoff's zone of constant pressure and linear cavitation."[28]

Figure 5 is an example of the approximation used for the separation delay with respect to the steady state separation location, i.e. the RHS of Equation (19).
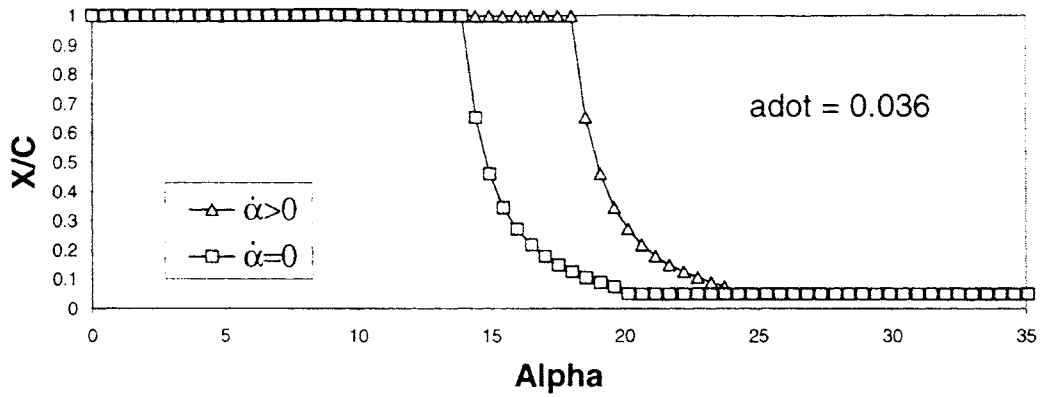
Figure 5. Delay in steady state separation due to α and τ_1.

The actual delay can be seen in Figure 6, with the inclusion of the rate of change in separation position, $(-\tau_1 dx/dt)$, with varying magnitudes of τ_1 into equation (19).
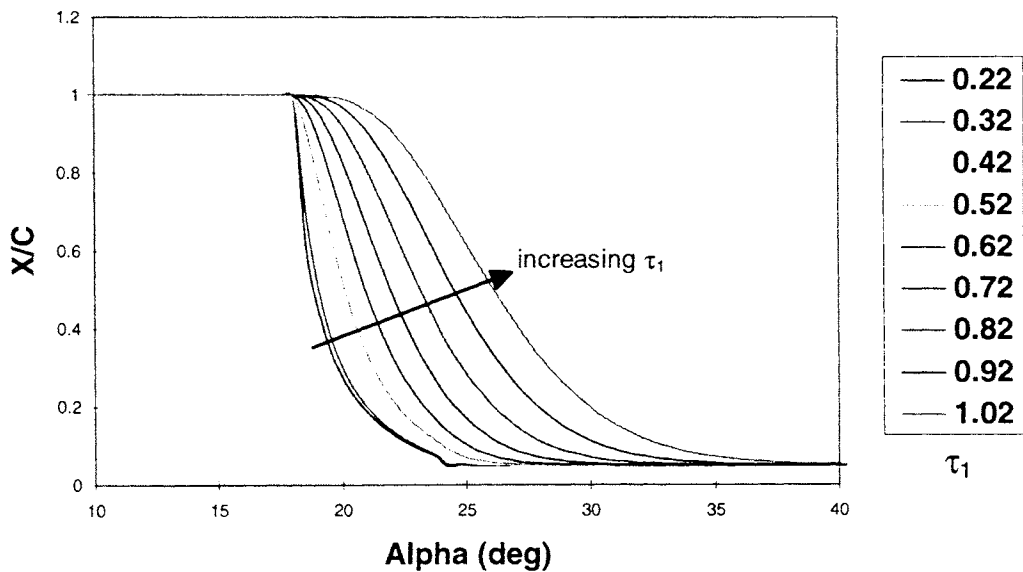
Figure 6. Actual separation delay with varying τ_1 as a function of α.

2.8 Kinematic Considerations

21

When treating time dependent motions of bodies, it is useful to describe the unsteady motion of the surface of which the "zero normal flow" boundary condition is applied in a body fixed coordinate system, as in Figure 1. The motion of this origin of the body fixed coordinate system is then prescribed to move in an inertial frame of reference and is assumed to be known. In other words, the steady form of the equations to solve take the form, for panel 1:

$$\sum_{j=1}^{n} (u, w)_j \cdot \hat{n}_1 = -(u_\infty, w_\infty) \cdot \hat{n}_1 \qquad (20)$$

With the addition of arbitrary pitching motion, an inertial reference frame coordinate system is established that is stationary while the airfoil is considered to move at a velocity (X_0, Z_0) and to pitch at some Θ about some arbitrary axis, such that the airfoil moves at a constant forward speed in the negative x direction, U_∞, and oscillates at a frequency, ω, about the y-axis.

$$\dot{X}_0(t) = -U_\infty$$
$$\dot{Z}_0(t) = 0 \qquad (21)$$
$$\Theta(t) = \sin(\omega t)$$
$$\dot{\Theta}(t) = \omega \cos(\omega t)$$

So with respect to the body fixed frame, the velocity seen by the airfoil becomes:

$$U(t) = \cos(\Theta)U_\infty - \dot{\Theta}\, dz$$
$$W(t) = \sin(\Theta)U_\infty + \dot{\Theta}\, dx \qquad (22)$$

22

where dx and dz represent the moment arm to the center of rotation. Therefore, with the inclusion of arbitrary unsteady motion and the effect of the unsteady wake's influence (u_{wake}, w_{wake}), the right hand side becomes, on panel 1:

$$RHS_1 = -\left[\left(U(t) + u_{wake}\right)\hat{i} + \left(W(t) + w_{wake}\right)\hat{k}\right] \cdot \overset{\wedge}{n_1} \tag{23}$$

where

$$\left(u_{wake}, w_{wake}\right)_1 = \sum_{j=1}^{t-\Delta t} \left(u, w\right)_j \tag{24}$$

induced on panel 1 from previously shed discrete vortices, where the induced velocities from a discrete vortex are given by:

$$\begin{aligned}
u &= \frac{\Gamma}{2\pi}\frac{z - z_0}{\left(x - x_0\right)^2 + \left(z - z_0\right)^2} \\
w &= \frac{-\Gamma}{2\pi}\frac{x - x_0}{\left(x - x_0\right)^2 + \left(z - z_0\right)^2}
\end{aligned} \tag{25}$$

with each vortex center located at (x_0, z_0).

2.9 Solving the System of Equations

The previous modelling setup the following system of equations, for one airfoil, that have the following number of boundary conditions: N wing panel flow tangency conditions, 2 Kutta conditions for the two separation points, and 1 Kelvin condition for

circulation. The unknowns for the system are: N wing source panel strengths (σ_N), 1 wing vortex panel strength (γ_{wing}), and 2 nascent wake vortex strengths (Γ_{sep}, Γ_{te}) that are separated at that time step. Accordingly, everything done up to this point boil down to one system of equations. The assembled system of equations can be seen in Equation 26.

$$
\left(
\begin{array}{cccc|ccc}
a_{1,1} & a_{1,2} & \dots & a_{1,n} & a_{1,wing} & a_{1,te} & a_{1,sep} \\
a_{2,1} & a_{2,2} & \dots & \dots & \dots & \dots & \dots \\
\dots & \dots & \dots & \dots & \dots & \dots & \dots \\
a_{n,1} & \dots & \dots & a_{n,n} & a_{n,wing} & \dots & a_{n,sep} \\
\hline
b_{1,1}+b_{n,1} & b_{1,2}+b_{n,2} & \dots & Kutta\ 1 & b_{1,wing}+b_{n,wing} & \dots & b_{1,sep}+b_{n,sep} \\
0 & 0 & \dots & Kelvin & \sum_{i=1}^{n} dl_i & 1 & 1 \\
b_{s,1} & b_{s,2} & \dots & Kutta\ 2 & b_{s,wing} & \dots & b_{s,sep}
\end{array}
\right)
\left(
\begin{array}{c}
\sigma_1 \\
\dots \\
\dots \\
\sigma_n \\
\gamma_{wing} \\
\Gamma_{te} \\
\Gamma_{sep}
\end{array}
\right)
=
\left(
\begin{array}{c}
RHS_1 \\
\dots \\
\dots \\
RHS_n \\
RHS_{n+1} \\
\sum_{i=1}^{t-\Delta t} \Gamma_i \\
RHS_{n+3}
\end{array}
\right)
$$

(26)

where RHS_{n+1} and RHS_{n+3} are given as:

$$
RHS_{n+1} = - \sum_{t=1}^{t-\Delta t}(u, w)_{wake_1} \cdot \hat{t}_1 - \sum_{t=1}^{t-\Delta t}(u, w)_{wake_n} \cdot \hat{t}_n
$$
$$
- (U_\infty, W_\infty) \cdot \hat{t}_1 - (U_\infty, W_\infty) \cdot \hat{t}_n
$$

(27)

$$
RHS_{n+3} = - \sum_{t=1}^{t-\Delta t}(u, w)_{wake_s} \cdot \hat{t}_s - (U_\infty, W_\infty) \cdot \hat{t}_s
$$

(28)

The system given by Equation 26 is solved simultaneously at each instant in time resulting in the strengths of the source panels, the bound vortex strength, and the strengths of the two nascent shear layer vortices. The position of the nascent vortices are iterated until their position becomes relatively fixed with respect to the change in the angle of the velocity vector calculated at their respective centers at each iteration. This

iteration is performed by an inner loop which moves the nascent vortex at the trailing edge a distance of $(u,w)/(0.1*dt)$. The vortex's new position is then compared with it's old position until the percent error is within 1×10^{-6} to ensure relative stability in it's change in iterated position. The shed wake vortices are then moved according to their local velocity, evaluated at their respective centers, multiplied by the time step. This process can be seen schematically in Figure 7.
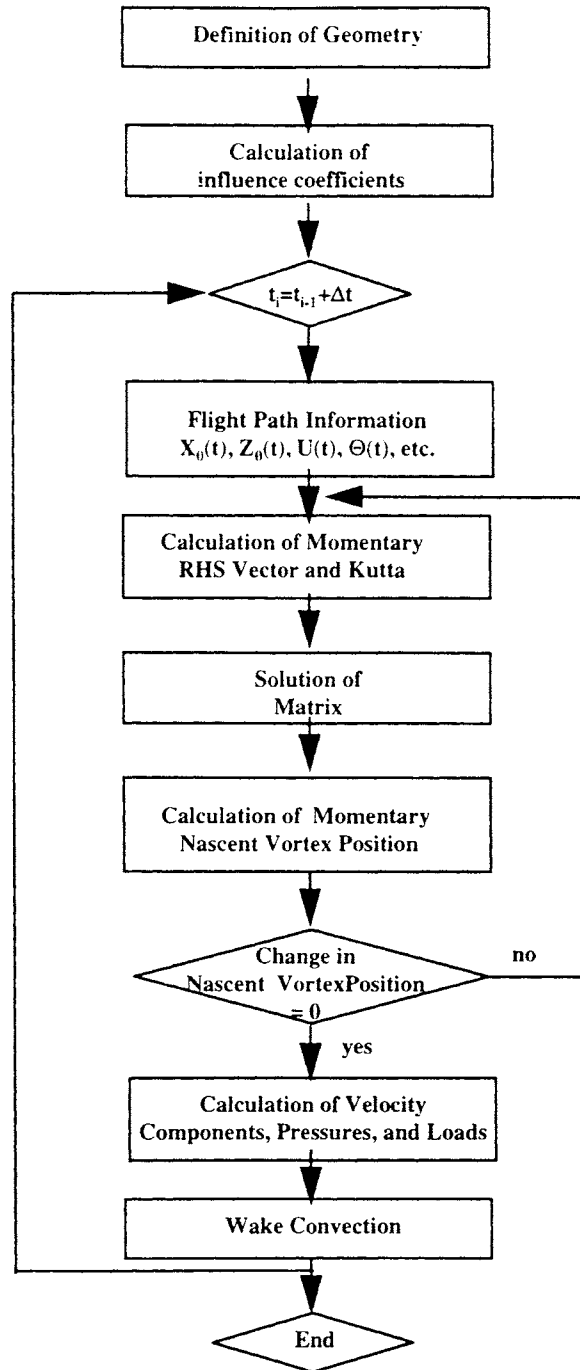
Figure 7. Schematic flow chart for the numerical solution of the unsteady airfoil.

The addition of a second airfoil adds to the system of equations another N_{tail} flow tangency conditions, one Kutta condition for the trailing edge, and one Kelvin condition for the circulation generated by the second airfoil. This system is solved simultaneously as before.

Typical run times for the wing and tail configuration for 200 nondimensional time steps were about 20 minutes on a time shared RS6000-320. Whereas for 100 nondimensional time steps the run time was only about 5 minutes. This is due to the heavy bookkeeping required to keep track of the coordinate positions of each individual shed vortex at each instant of time.

2.10   Pressures & Loading

The pressure coefficients are obtained using the unsteady Bernoulli equation:

$$C_p = 1 - \frac{V^2}{V_\infty^2} - \frac{2}{V_\infty^2} \frac{\partial \Phi}{\partial t} \qquad (29)$$

where V is the total velocity at a point and is known.

The calculation of the change in the potential with respect to time ($\partial\phi/\partial t$) is slightly more involved. As mentioned previously, the gradient of the potential is the velocity. So then, the integration of the velocities, which can be found at any point, yields the potential. Therefore, starting the integration at a distance that approximates infinity, where we know the velocities will be zero from the boundary condition of equation 6, we can thus determine the potential at any point off the airfoil by integrating the velocities starting the integration at approximately infinity. Once at the airfoil, the potential jump across a constant strength vortex panel is given by:

$$\Delta \Phi(x) = \Gamma(x) \tag{30}$$

i.e. the potential jump across a constant strength vortex panel is the difference in Φ just above the panel to just below the panel. Also note that the potential jump across a constant strength source panel is zero. The change in Φ with respect to time on one panel is then:

$$\frac{\partial(\Delta \Phi(x))}{\partial t} = \frac{\partial(\Gamma(x))}{\partial t} = \frac{(\gamma_t - \gamma_{t-\Delta t}) \cdot dl}{\Delta t} \tag{31}$$

where γ is the wing vortex panel strength, Γ is the total wing panel circulation (i.e. $\gamma*dl$), dl is the wing panel length, t and t-Δt are the present and previous time steps respectively. Consequently, by keeping track of the previous and present time steps potential and circulation values along some fixed line with respect to the body fixed coordinate system, the change in potential with respect to time can be found. For the entire wing surface, this equation is summed around the wing surface in the clockwise direction starting from the lower trailing edge panel adding in the change in potential off the airfoil determined from the integration scheme. Another potential jump is included in the sum, as it passes the secondary separation point, to represent the change in potential across the secondary shear layer. This jump is required since, for the integration/summation scheme to be correct, the region of integration must be a simply connected region to ensure a single valued result. This constraint is however manageable since the change in potential with respect to time across the shear layer is known and is equal to the change in vorticity with respect to time of the shear layer emanating from the separation point, i.e. the strength of the last shed vortex (γ_s)/Δt. Thus the total pressure coefficients and total lift and moment then become:

$$Cp_j = 1 - V_j^2 - 2 \cdot \sum_{i=1}^{j} \left\{ \frac{(\gamma_t - \gamma_{t-\Delta t})_i \cdot dl_i}{\Delta t} + \left[\frac{(\gamma_s)_t}{\Delta t} \right]_{i \geq s} \right\}$$

$$C_l = \sum_{i=1}^{N} Cp_i \cdot dl_i \cdot \cos(\theta_i - \alpha) \qquad (32)$$

$$C_m = \sum_{i=1}^{N} Cp_i \cdot dl_i \cdot \cos(\theta_i - \alpha) \cdot x_i$$

where j is the panel number and s represents the panel that separation occurs. Note that x_i is the moment arm to the center of pressure, which in this case is at c/4. The use of $\partial\Gamma/\partial t$ for $\partial\phi/\partial t$ is analogous to Sears'[13] representation of lift and moment using the change of vorticity of the bound vortex system with respect to time as the $\partial\phi/\partial t$ term. Also note that once the nascent vortices are shed their individual strengths are conserved. This stems from the vorticity transport equation:

$$\frac{D\zeta}{Dt} = \zeta \cdot \nabla \hat{q} \qquad (33)$$

For a two dimensional, inviscid, and incompressible flow this simplifies to:

$$\frac{D\zeta}{Dt} = 0 \qquad (34)$$

which is a good approximation for most high Reynolds number flows.

CHAPTER III

RESULTS

The rationale for the validation of the model begins with a single airfoil having separation only at the trailing edge to verify the impulsively started airfoil's unsteady sectional lift with theoretical solutions. Once the non moving attached flow has been investigated, analysis moves on to attached oscillatory motion comparing it with theoretical solutions. The process then goes on to add secondary separation at higher angles of attack to verify time averaged sectional lift and moment with experimental measurements, as well as adding a second airfoil to study the dynamic interactions between a two-dimensional wing and tail system with the separated wake. Finally, ramp motion from zero degrees to a maximum of sixty degrees angle of attack and allowing for separation is examined and compared with experimental data.

3.1 Unsteady Attached Flow

The unsteady attached flow case is a logical starting point for the validation of this model. The flow is only allowed to separate at the airfoil's trailing edge and is kept below its static stall angle of attack. The results are compared with classical solutions as well as other panel methods.

3.1.1 Impulsive Start

The model tested here was first verified with the Wagner[5] function (Fig. 8) using a NACA 0012 airfoil. The Wagner function is the time history of the normalized lift on an airfoil that has been started impulsively from rest at an angle of attack. Giesing's[24] results are also included to show the effect of thickness on transient lift. Note that this was done with the airfoil at an angle of attack of 5 degrees and no secondary separation occurs. The results show a transient lift lower than the Wagner case which is consistent with Giesing's results. Notice for the Wagner case, the lift at $t = 0+$ is exactly half of that of the steady-state lift, this is not due to the airfoil's circulatory lift but due to the acceleration portion of the lift that results from the change in the upwash ($\partial\phi/\partial t$). The magnitude of this force, from the fluid acceleration, decreases with the reduced influence of the starting vortex. At $t = 0$ when the airfoil was suddenly accelerated from rest the lift was infinite, due to this acceleration term. Also note the 12% thick NACA 0012 airfoil's lift lies in between the lift for an 8.4 % and a 25.5% airfoil.
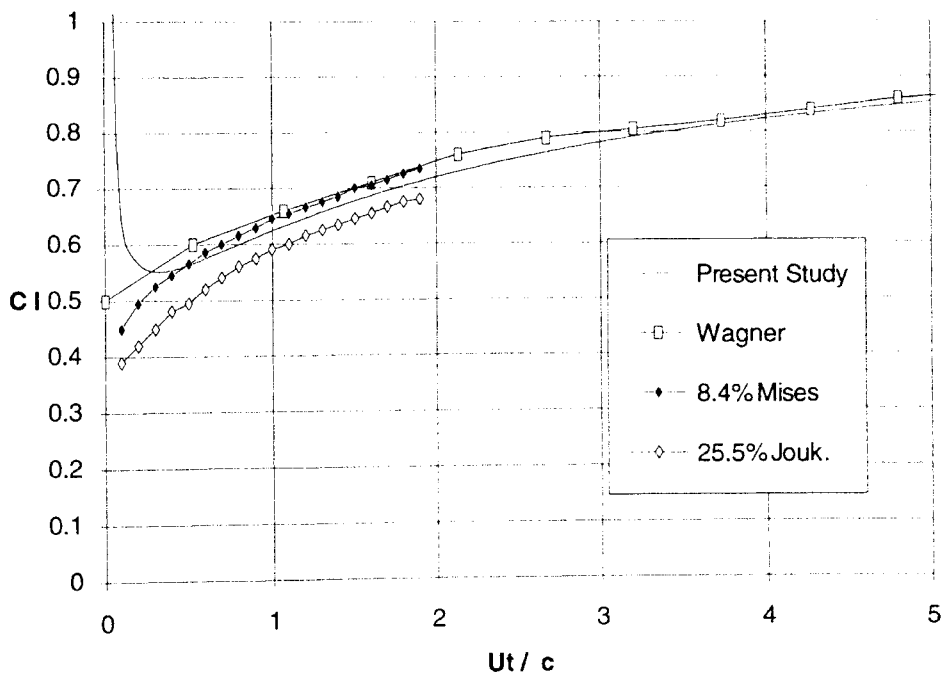
Figure 8. Comparison of calculated results with the Wagner[5] function and Giesing[24] exp. (dtU/c=.025).

The wake picture for this static impulsive start case can be seen in Figure 9. Notice the wake curl at the end of the wake from the induced effect of the other vortices. Note that all distances are nondimensionalized with the airfoil chord length. Also, shown in Figure 10, is the pressure coefficient distribution for several time steps. The unsteady data is compared with the steady state pressure coefficients and shows that the effect of the wake is to suppress the lift. As the airfoil sheds less vorticity through time, since the total circulation is conserved, and the distance of the airfoil to the initial starting vortex is increasing, its lift can be seen to increase, as seen in Figure 8 and 10. The airfoil geometry is also included to aid in the visualization of where the pressure coefficients reside relative to the airfoil. Notice the expected suction peak at the upper leading edge surface due to the increase in velocity of the flow traversing the upper leading edge contour.
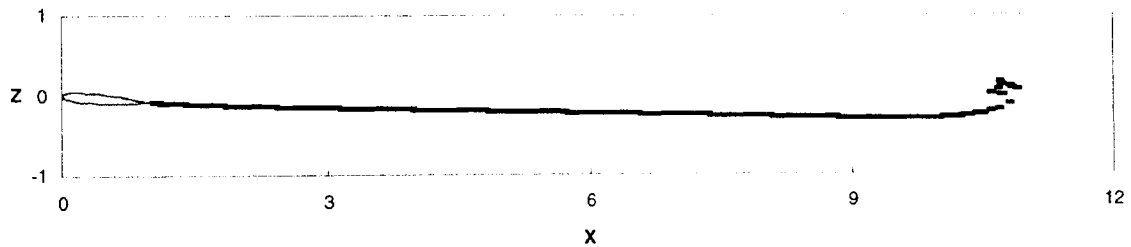
Figure 9. View of the shed wake behind an airfoil at 5 deg. for the Wagner case (dtU/c=.025).
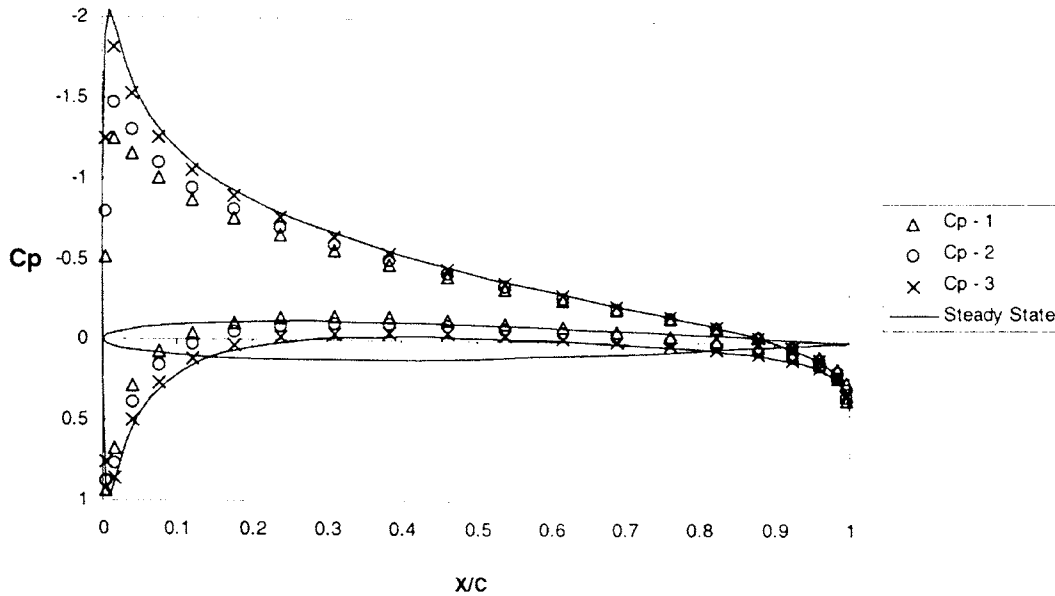
Figure 10. Comparison of pressure coefficient distribution with steady state behind an airfoil at 5 deg. for the Wagner case (dtU/c=.025).

The results from this simple first case of a static airfoil impulsively started show excellent agreement with theoretical results.

3.1.2 Oscillatory Motion

Airfoil motion is the next avenue to consider. Can the model continue to simulate expected results when airfoil motion is included? Oscillatory attached flow is compared to the theoretical solution of Theodorsen.[4] Figure 11 represents the lift coefficient of an airfoil oscillating about its midchord sinusoidally with a maximum amplitude of 5 degrees in angle of attack, at a reduced frequency, $(f_{red} = \omega c/V_\infty)$, of 1.0. Note that the lift in Fig. 11 is moving in a clockwise direction and can be considered to lead the oscillatory motion of the airfoil.

33

Figure 11. Comparison of the aerodynamic model's C_l with Theodorsen's solution pitching at a reduced frequency of 1.0.

Also, shown in Figure 12, is the moment coefficient about the midchord with respect to angle of attack for the same run as that of Figure 11. Note that for Fig. 12, the moment moves in a counter-clockwise direction and can be considered to lag the oscillatory motion of the airfoil from the energy dissipating damping effect due to the unsteady effects. The significance of this lag, from a stability perspective, is that a restoring moment is not always present during the sinusoidal motion. The data point in Figure 12 below the main group is the initial calculation at the first time step and stems from the initial influence of the starting vortex. The figures show very good correlation with the theoretical solutions keeping in mind that the Theodorsen function does not account for thickness effects.
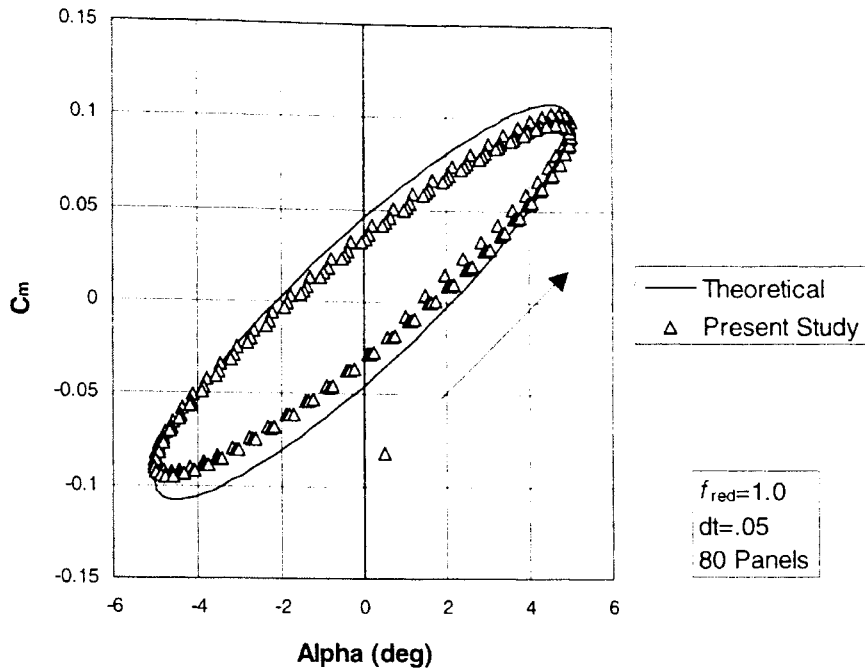
Figure 12. Comparison of the aerodynamic model's C_m with Theodorsen's solution pitching at a reduced frequency of 1.0.

The wake picture of the pitching airfoil is evident in Figure 13. Notice the shape of the wake resulting from the airfoil motion and the curl at the end of the wake from the strength of the initial starting vortex.
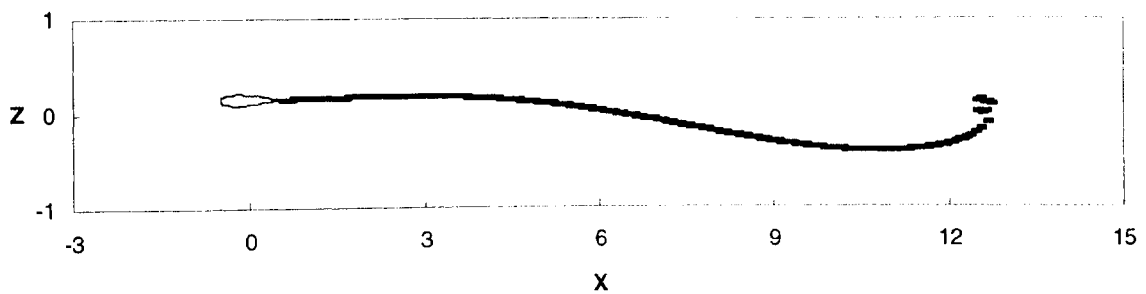
Figure 13. View of the shed wake behind an airfoil pitching at a reduced frequency of 1.0, at an amplitude of 5 degrees.

The pressure coefficient distributions of the pitching airfoil is shown in Figure 14. For this particular figure, the pressure coefficients are shown for two moments in time when the airfoil is momentarily at approximately an angle of attack of zero degrees, once when the airfoil's pitch rate is positive and once when the airfoil's pitch rate is negative. The top surface relative to the bottom surface for the two moments in time can be compared. Notice that the pressures for the top surface pitching up is greater than that for the top surface pitching down. This data is also compared with the steady zero angle of attack lift. Thus showing the unsteady effects of the airfoil motion to the pressure coefficient distribution is distinct and results in the lift seen in Figure 11.
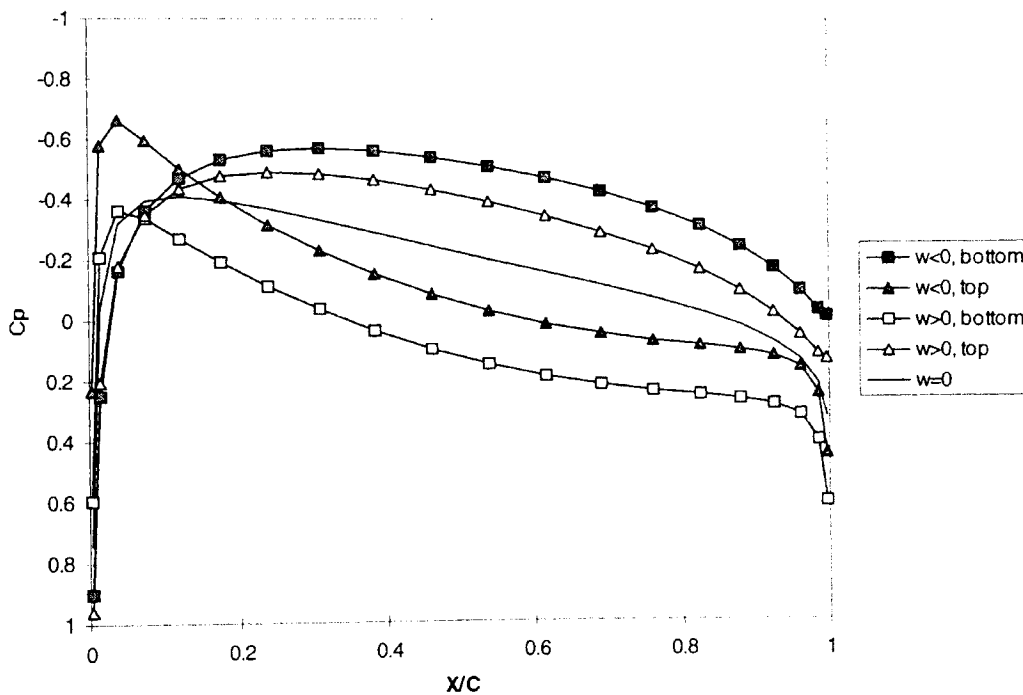
Figure 14. Comparison of the pressure coefficients for an airfoil at an angle of attack of 0 degrees pitching at a reduced frequency of 1.0 along with the steady pressure coefficients at zero degrees.

Further analysis was done into a plunging oscillatory motion as can be seen in figures 15 - 18. For this test, the airfoil was moved sinusoidally as before, with the same

reduced frequency of 1.0, except in this case, rather than a pitch motion, the airfoil was put through a plunging motion, to a maximum amplitude of h/c=0.15. In figure 15, the lift can be seen to move in a clockwise direction as before, but the slope of the ellipse's major axis is negative, rather than a positive slope that was seen for the pitching case. This can be attributed to the physical motion change that was introduced. Also, notice in Figure 18, where the drag coefficient is plotted versus nondimensional plunging height, that the drag coefficient becomes slightly positive for a portion of the motion due to the orientation of the relative wind. In other words, a component of thrust is obtained for a two dimensional unsteady inviscid flow analysis, this is in contrast to a two dimensional steady flow analysis that would result in the drag coefficient being zero. Again, the numerical results follow that of the theoretical solutions.
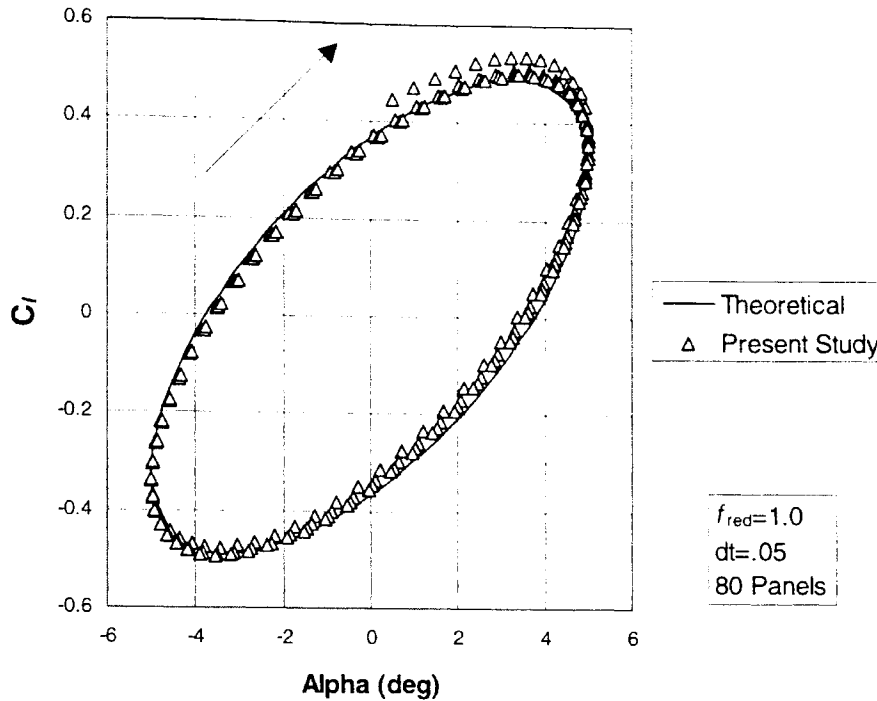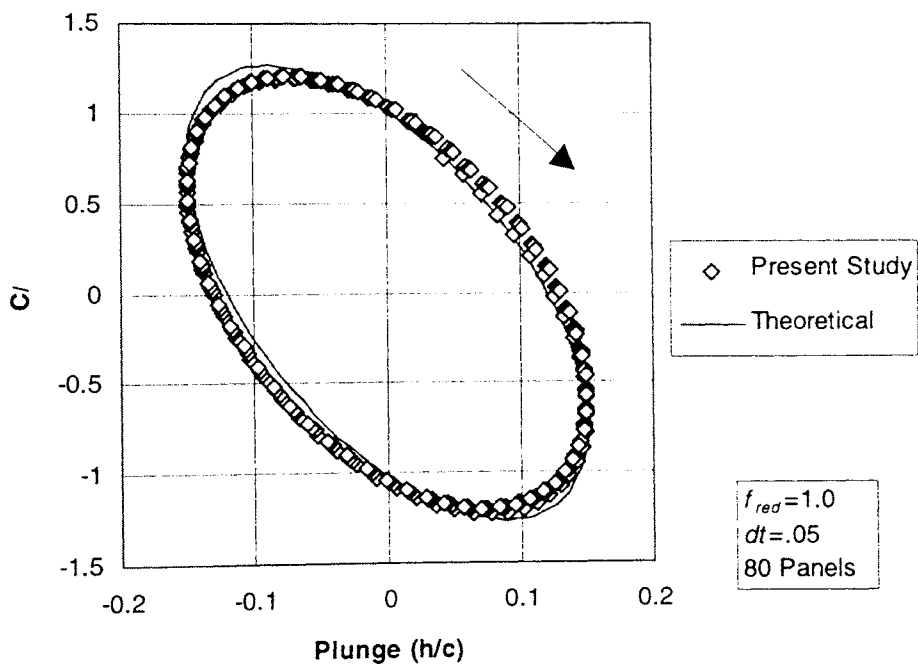

Figure 15. Comparison of the aerodynamic model's C_l with
Theodorsen's solution for plunging at a reduced frequency of 1.0.
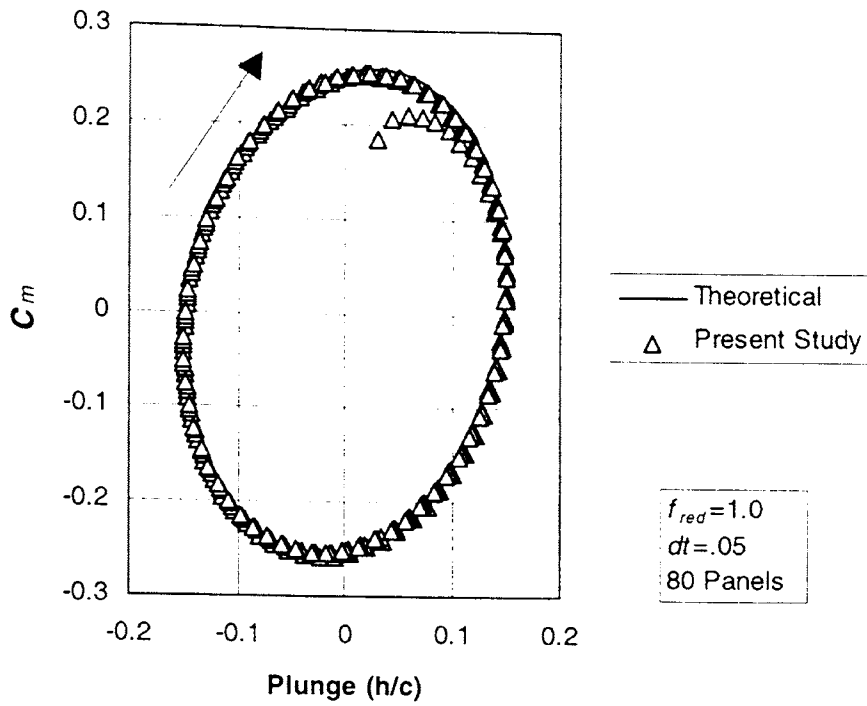
Figure 16. Comparison of the aerodynamic model's C_m with Theodorsen's solution for plunging at a reduced frequency of 1.0.
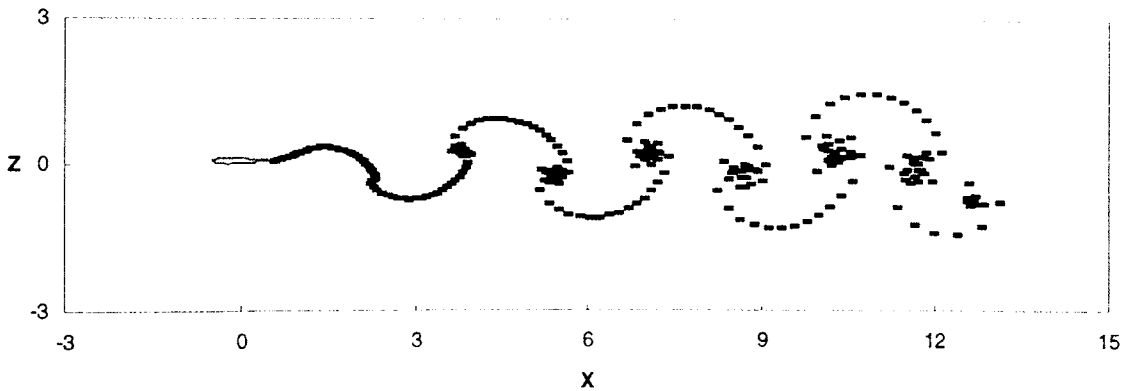
Figure 17. View of the shed wake behind an airfoil plunging at a reduced frequency of 1.0, at an amplitude of 0.15 h/c.

38
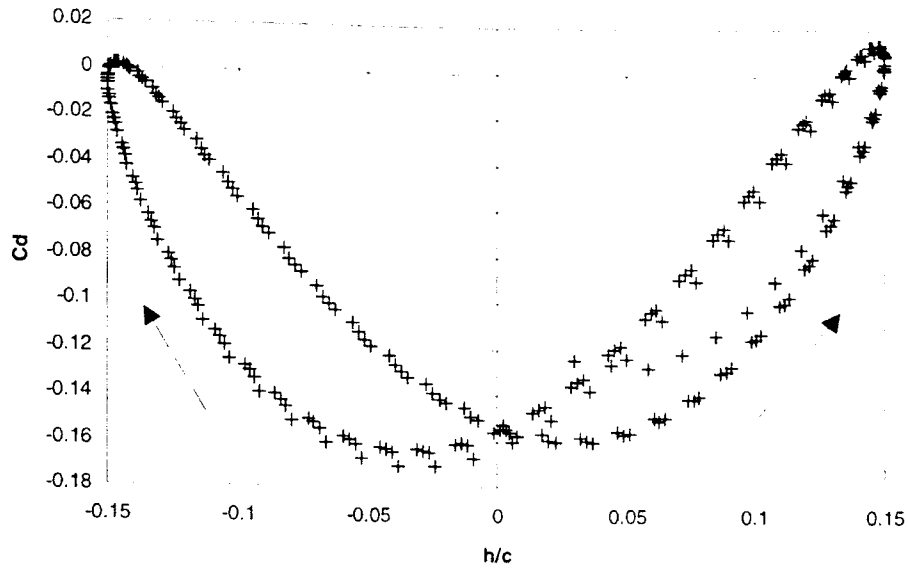
Figure 18. View of drag coefficient of an airfoil plunging at a reduced frequency of 1.0, at an amplitude of 0.15 h/c.

3.2 Separated Flow

3.2.1 Static Angle of Attack

With the unsteady model validated and appearing to be performing adequately, a series of tests were performed to ascertain the model's feasibility towards separated flow. This was done by first analyzing the model's output for a static airfoil at various angles of attack in regards to its time averaged lift and moment coefficients. Also, for the static case, a tandem airfoil was included as well to examine the wake shedding's effect of a stalled airfoil on a second airfoil and the resulting lift and moment for two different tandem airfoil configurations. Finally, several dynamic stall tests were done to test the limits of the model with respect to the rate of change of angle of attack as well as the performance of the state-space representation of the separation point transition.

First the airfoil was positioned at various angles of attack and constrained to separate at a point dictated by Figure 19 from Katz.[17] Note that the separation point of the present study is assumed to be at 5% chord at angles of attack above 20 degrees. The time averaged lift and moment coefficients were then obtained (Figs. 20 & 21). The data obtained is compared with experimental work done by Critzos[29] using a NACA 0012 airfoil from an angle of attack of 0 to 85 degrees. Notice in figure 20 the initial increase in lift before separation sets in, the sharp drop off as stall is reached, a gradual increase in lift reaching a second maximum at 45 degrees, and finally a gradual decrease up to 85 degrees angle of attack. In Figure 21, notice the initial zero sectional moment until stall is reached and the gradual increase in the restoring moment as the angle of attack is increased. The lift and moment figures compare exceptionally well with the experimental data over the entire range tested.
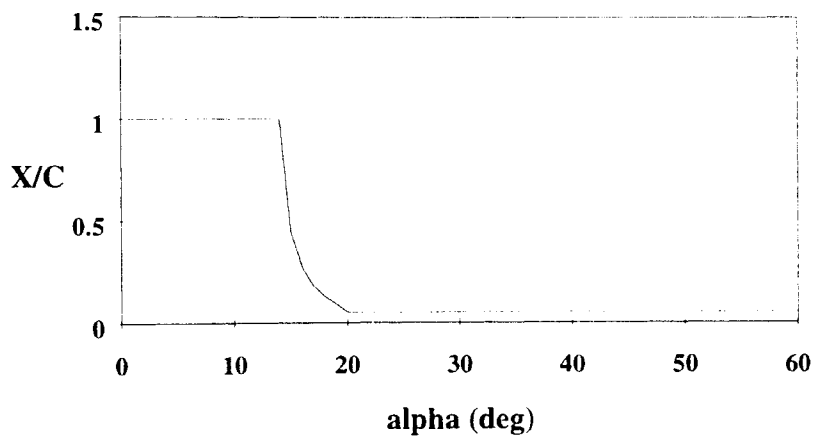
Figure 19. The assumed steady position of the separation point for a NACA 0012 airfoil.[17]
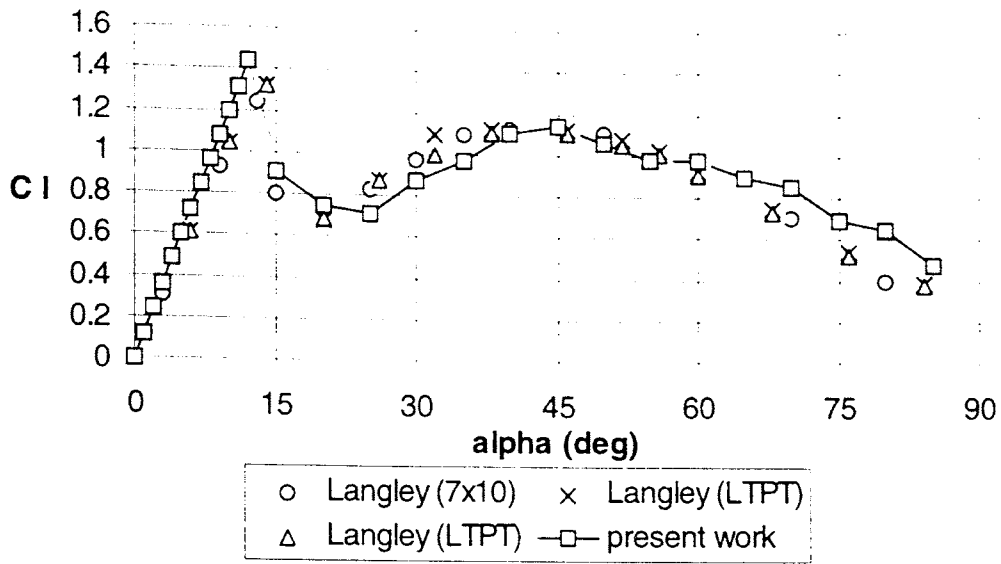
Figure 20. Comparison of sectional lift coefficient with experimental data on a NACA 0012 from Critzos.[29] (ref. 6 of ref. 29)
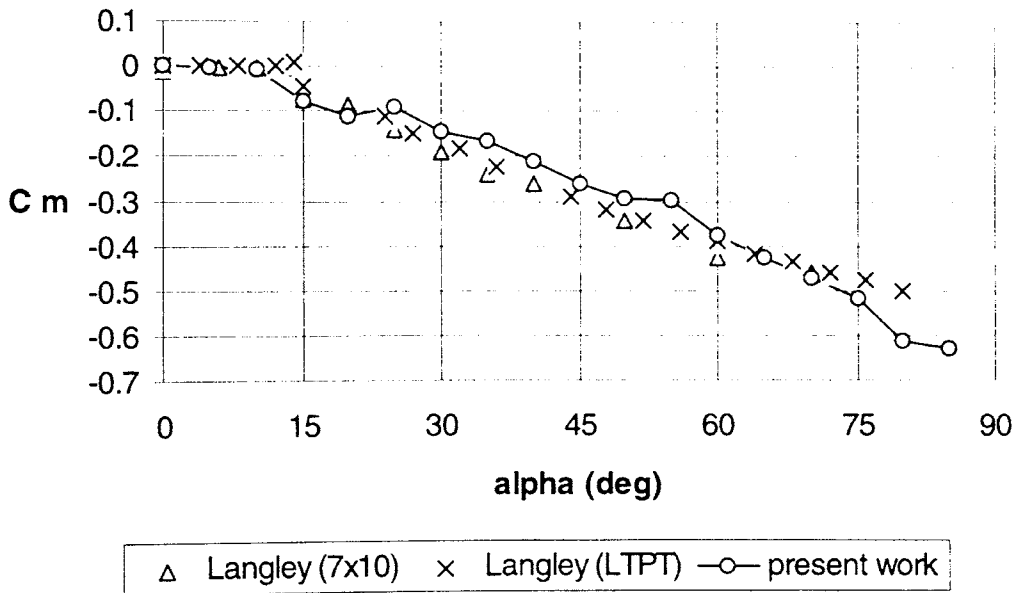
Figure 21. Comparison of sectional moment coefficient with experimental data on a NACA 0012 from Critzos.[29] (ref. 6 of ref. 29)

Particle tracking of discrete vortices was also accomplished by storing each vortex's position through time. This was done for the purpose of animating the flowfield

41

through time to show the movement of the shed vortices in order to visualize the wake character. The periodic wake shedding behind an inclined airfoil with separation at 5% chord is shown in Figure 22. The figure shows the interactions between the upper and lower shed wakes are highly prominent as well as a well defined oscillatory pattern. The oscillatory wake shedding shown is consistent with flow visualization studies of separated flow on bluff bodies, as in the familiar Karman vortex street. However Figure 22 does not show the shed wake's influence on the velocity field. Figure 23 shows a representative picture of the shed wake's influence on the velocity field. Here it can easily be seen how the wing's alternate wake shedding affects the velocity field. Also notice in Figure 23 the low energy region and the reverse flow on top of the airfoil behind the separation point due to the enforced stagnation point.
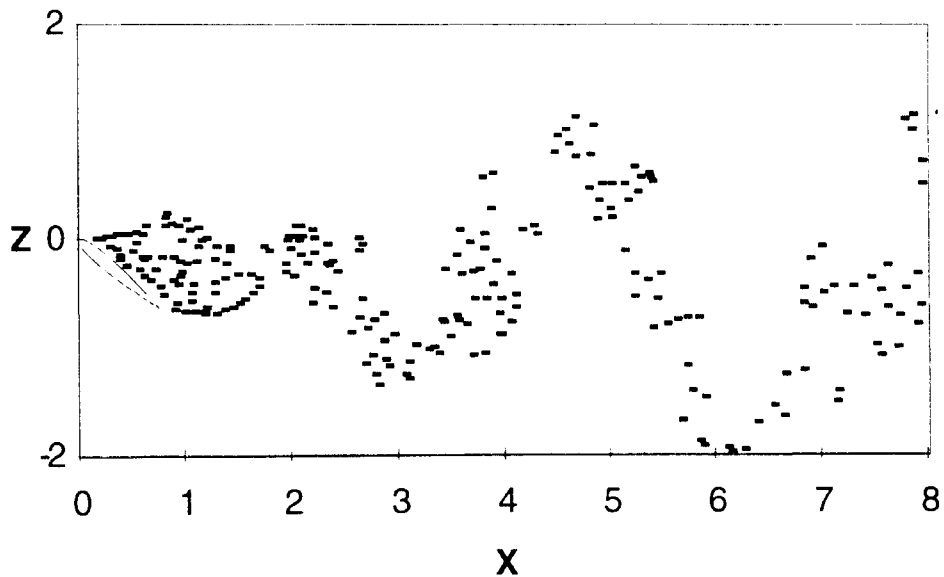
Figure 22. Picture of the shed wake of the wing at 20 sec, a = 40 deg (dtU/c=0.1)

Figure 23. Velocity vectors of the wing at 20 sec, $\alpha = 40$ deg (dtU/c=0.1)

The oscillations are also apparent in Figure 24 which shows the time dependent sectional lift and moment coefficients for an angle of attack of 40 degrees. Again, notice the oscillatory nature of the lift which is primarily related to the shedding pattern shown in Figures 22 & 23. This can be attributed to the relative proximity of the wake's peaks and valleys with respect to the wing and their respective induced velocities on the wing. The figure is consistent with experimental observations. The data in Figure 24 represents an example of what was time averaged at a particular angle of attack for Figures 20 and 21. Note that time averaging was done for the period between 10 and 20 non-dimensional seconds where the impulsive start effects have been overcome and the system has become relatively stabilized.
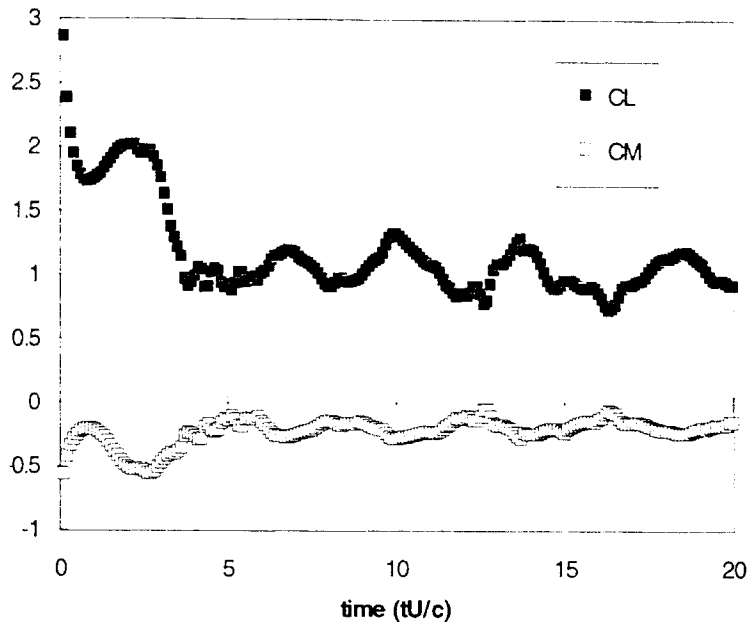
Figure 24. Sectional lift and moment coefficients vs. nondimensional time for the wing $\alpha = 40$ deg.

3.2.2 Tandem Airfoils

The interactions that result from a tandem airfoil configuration, i.e. wing and tail, with one airfoil stalled is next to study. Accordingly, the mutual effects of the wing and the tail on the total time averaged lift and moment due to the separated flowfield with reference to the position of the tail are analyzed.

The tail was added and positioned at heights of zero (h=0) and one (h=1) chord length relative to the chord line to study the effects of the tail on the shed wake as well as its' effects on the wing. Figure 25 shows another particle tracing of discrete vortices for both the wing and tail with the tail at a height of one wing chord length and a distance downstream of one wing chord length. Here it can be seen that the effect of the tail on the wake is to break up the wing's oscillatory wake pattern making it much more chaotic in nature.

44
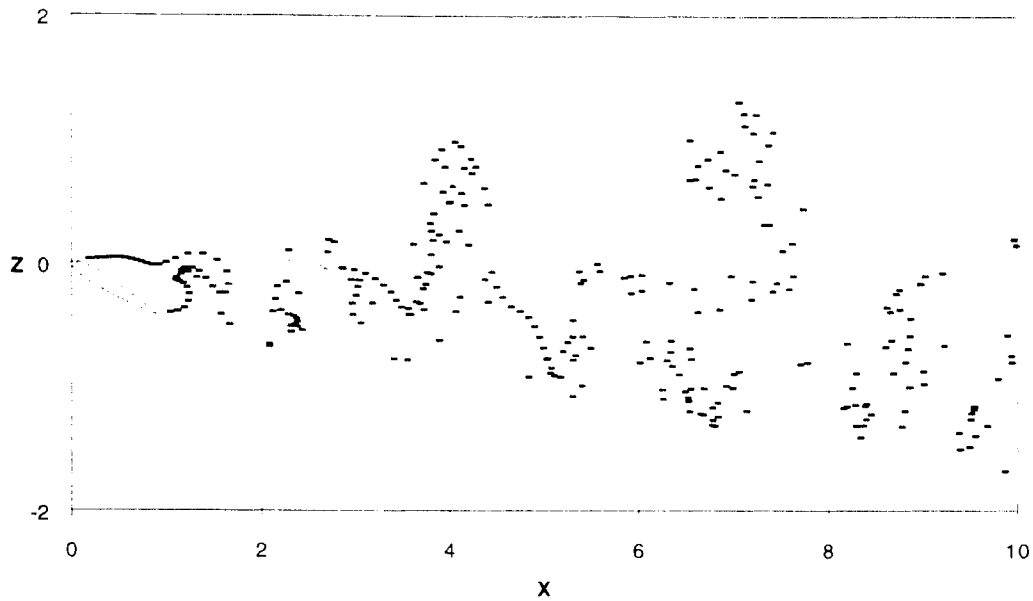
Figure 25. Picture of the wing, tail, and shed wake at 20 sec, α_w = 25 deg, α_t = 13 deg (dtU_∞/c=0.1)

However the figure does not show the effect the wake has on the velocity field so Figures 26 (a) and (b) show representative pictures of the wing, tail, and shed wake's influence on the velocity field. The vector fields also show the instantaneous effective angle of attack of the tail. The reader should notice, for the tail high case (h=1), the upwash on the tail due to the wing's trailing edge wake and the oncoming downwash from the wing's upper separation wake, thus magnifying the oscillatory moment on the wing from the tail with respect to time due to the rapidly changing velocity field. Whereas, for the tail low case (h=0), the downwash on the tail is relatively constant since the tail witnesses a less oscillatory velocity field thereby making its influence on the total lift and moment much less oscillatory.
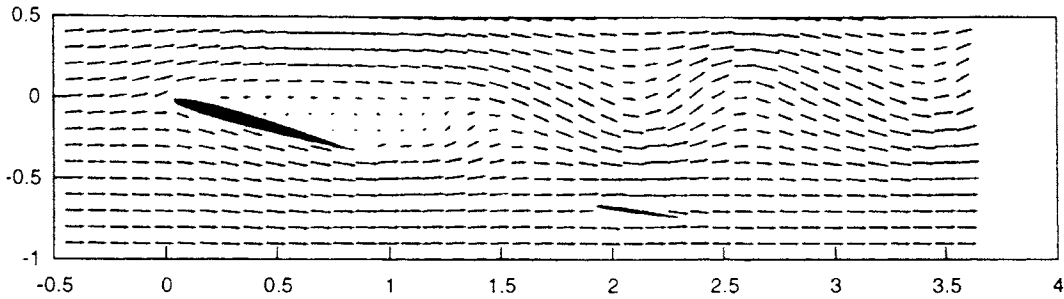
Figure 26 (a). Velocity vectors of the wing and tail at 20 sec, $\alpha_w = 25$ deg, $\alpha_t = 13$ deg (dtU/c=0.1), tail low
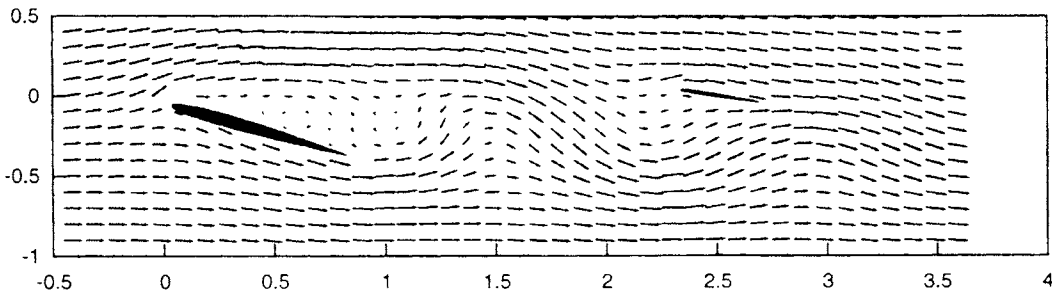
Figure 26 (b). Velocity vectors of the wing and tail at 20 sec, $\alpha_w = 25$ deg, $\alpha_t = 13$ deg (dtU/c=0.1), tail high

The result of the wake's oscillatory pattern can be seen graphically in Figure 27 where the time dependent sectional lift and moment coefficients are shown for the tandem airfoil configuration, tail low, h=0 and tail high, h=1. Note here that the total sectional moment coefficient for the tail high case is occasionally positive, due to its position in the wing's wake, while for the tail low case the moment remains negative through time. From a stability standpoint, this characteristic of a positive moment, corresponding to a pitch up moment, is very undesirable since the would result in an increasing pitch up requiring more input force to control the instability. Thus the difference between the characteristics of the tail low and tail high cases in terms of the lift and moment oscillations are primarily due to the contributions from the tail. Note that, at the present time, the tail flow is assumed to be attached. So for the present tests the angle of incidence of the tail with respect to the freestream is kept below 13 degrees, the static

46

stall angle of attack. This assumption is a first approximation since it is understood that, with a rapidly changing velocity field, the secondary separation point criteria for the tail flow can not be based on single airfoil experimentation due to the added induced velocities from the wing on the tail and the resulting dynamic variation of the effective angle of attack of the tail.
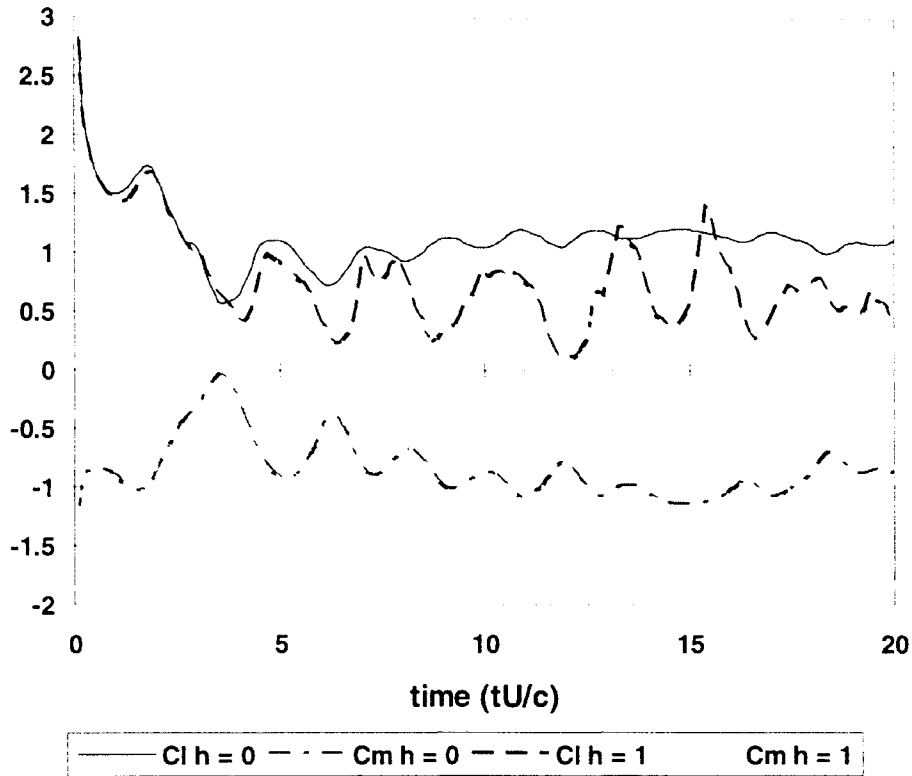
Figure 27. Sectional lift and moment coefficients vs. nondimensional time for the wing and tail configuration. α_w = 25 deg., α_t = 13 deg.

The total wing and tail time averaged sectional lift and moment coefficients are shown in Fig. 28. Note that when the configuration is pre-stall the trim point for the system is roughly at 12 degrees angle of attack for both tail high (h=1) and tail low (h=0) cases. However when the configuration is post-stall, the tail high case has multiple trim points from angles of attack of 15 to 18 degrees. Whereas the tail low case has only the

one post-stall trim point at 15 degrees angle of attack. This is probably simply due to the fluctuating airmass traversing the tail high configuration, thereby making the relative angle of attack fluctuate as well, moving the trim point accordingly. Whereas for the tail low case, a more steady flow is encountered by the configuration. In other words, even though these trim points are obtained from time averaging, the net effect of the flowfield seen by the high tail is qualitatively different than that seen by the low tail. It is interesting to note that the wing and tail system show similar trends in lift to that of single airfoil experimental data such as Critzos.[29] The existence of multiple trim points is consistent with results obtained by Stengel[30]for a full scale high wing aircraft.
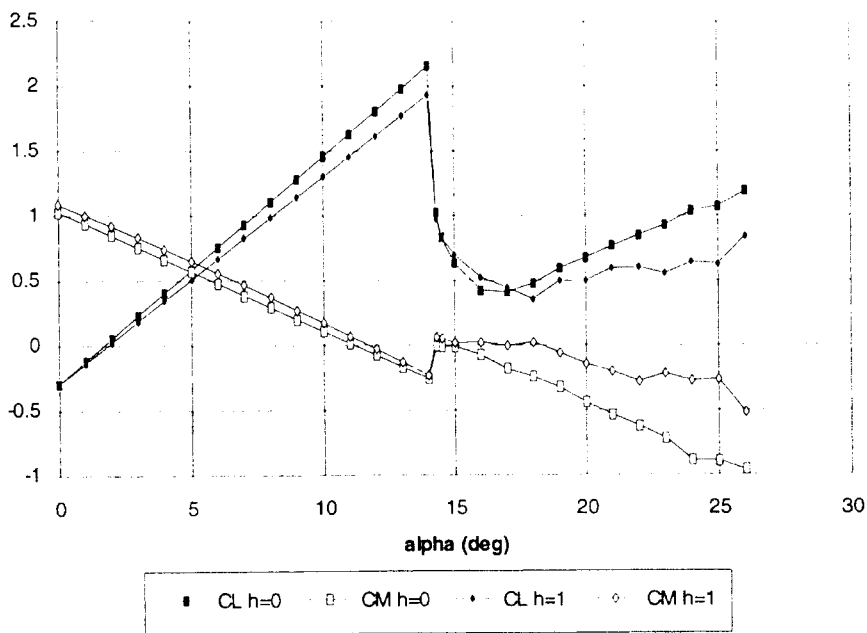
Figure 28. Time averaged sectional lift and moment coefficients for the
wing and tail configuration

3.2.3 Ramp Motion

Now, with static separation validated, separated ramp motion can be analyzed to see if we can model unsteady separated flow using a dynamic stall case with fully

unsteady boundary conditions. This particular test should show the significance of the model towards dynamic stall as well as the effectiveness of the state variable approach on modeling the separation point transition process.

For ramp motion, a NACA 0015 airfoil is impulsively started from rest at an angle of attack of 0 degrees. The airfoil rotates about the midchord at a constant nondimensional pitch rate, ($\dot{\alpha}_{nd}=\dot{\alpha}c/2V_{\infty}$), up to some large angle of attack. The upper separation point is initially 3 panels upstream from the trailing edge panel since two separate Kutta conditions cannot be enforced on or adjacent to each other. If they were enforced at the same panel location the effect would be to over constrain the system of equations, specifically, both Kutta conditions enforcing the same panels. The separation point then transitions up the airfoil per the separation model of equation 19. Figure 29 shows the numerical results plotted along with experimental results obtained from Jumper.[27] For the particular test cases of relatively low rates of change of angle of attack the parameters used from equation 19 are, $\tau_1=1.92$ and $\tau_2=0.3$. Notice that although the magnitudes of the lift are larger than those obtained experimentally, the trends are quite similar. The stall is delayed to a higher angle of attack for a greater rate of change of angle of attack as expected from the experimental results of Jumper. Also, for the moment coefficients in Fig. 30, the magnitudes differ somewhat but, comparing the experimental values, one can easily see the same similar trend between the experimental and numerical results.
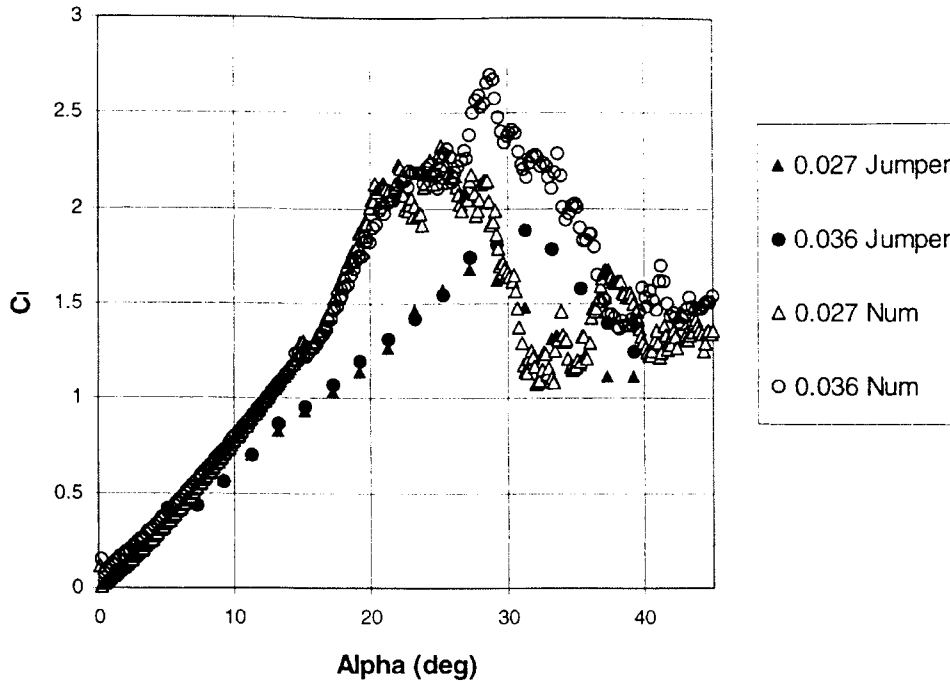
Figure 29. Comparison of the aerodynamic model's C_l with experimental data from Jumper[27] for ramping motion.
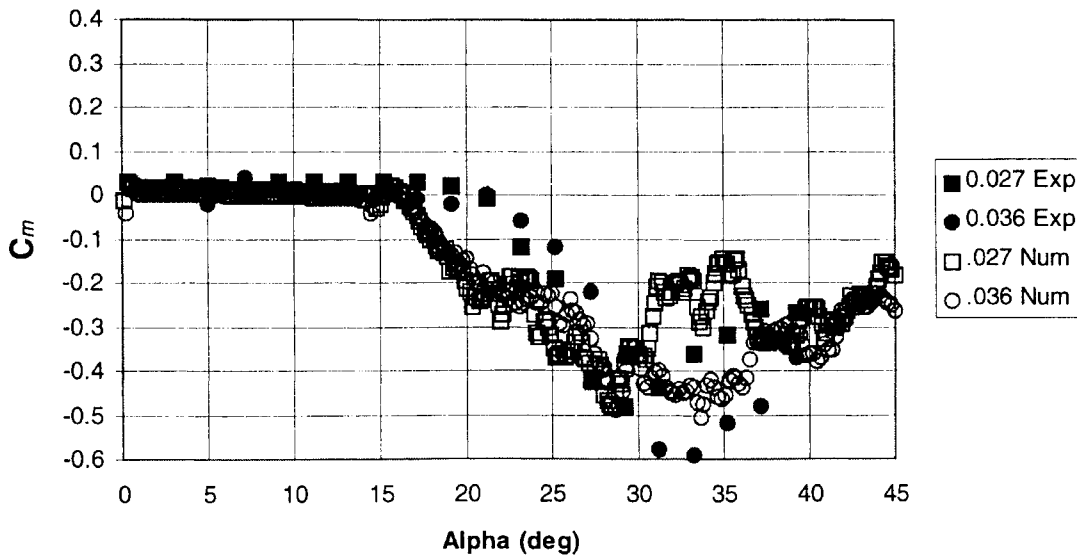
Figure 30. Comparison of the aerodynamic model's C_m with experimental data from Jumper[27] for ramping motion.

50

Experimental results from Helin[31] as well as computational results from Huyer[20] were also obtained and compared with this computational model in Figure 31. In this experiment, the airfoil is pitched at the midchord at a constant rate of 0.2, a much higher rate than that of Jumper, from zero degrees angle of attack. The pitching was then stopped at 5.2 nondimensional time units, corresponding to an angle of attack of 60 degrees, where the flowfield was then allowed to evolve. Lift coefficients exhibit an increase in magnitude during airfoil pitch up. A maximum lift coefficient of 2.75 was observed at 2.8 nondimensional seconds. Experimentally, two peaks were seen for maximum C_l with $C_{lmax} = 2.3$ seen at 3.0 nondimensional seconds. Direct comparisons with experimental data show the current numerical technique slightly over predicts lift during pitch up by approximately 8% and over predicts the maximum peak lift by approximately 12%. Also, the second sharp lift peak obtained numerically is approximately 60% greater than that obtained experimentally. Also, the present study compares well to that of the more complex simulation done by Huyer. [20]
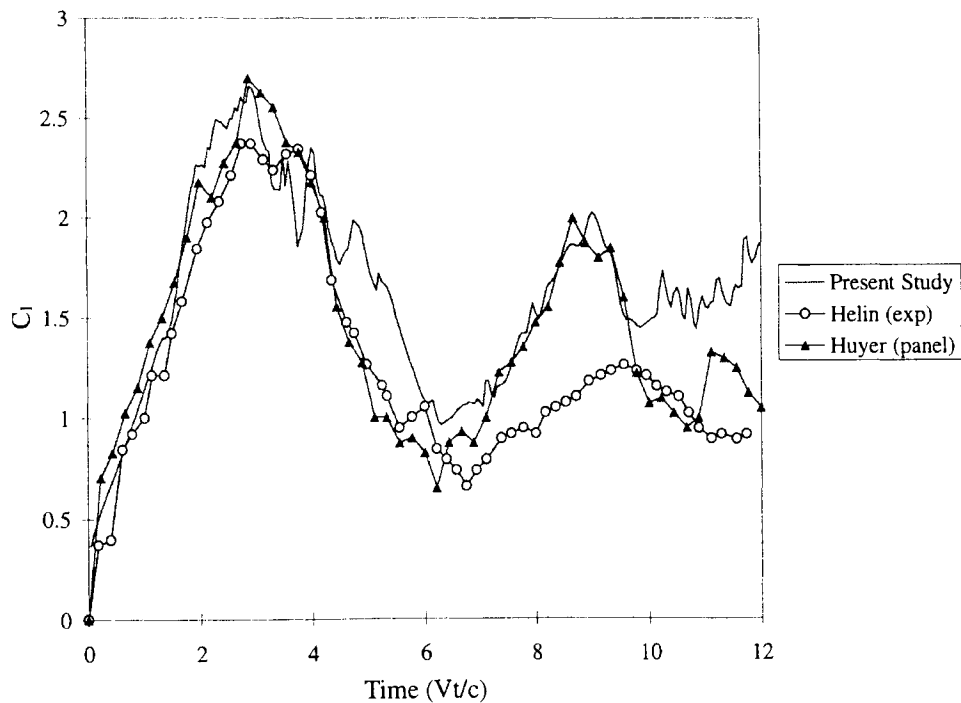
Figure 31. Constant pitch up ($\alpha_{nd} = 0.02$) stopping at 5.2 nondimensional seconds compared with Helin[30] experimental results.

The wake for this pitch up and hold case is shown in Figure 32 as a time history. Here again the alternate wake shedding pattern is apparent. Notice the upper separation point transition up the airfoil, then build to a large leading edge vortex before shedding.
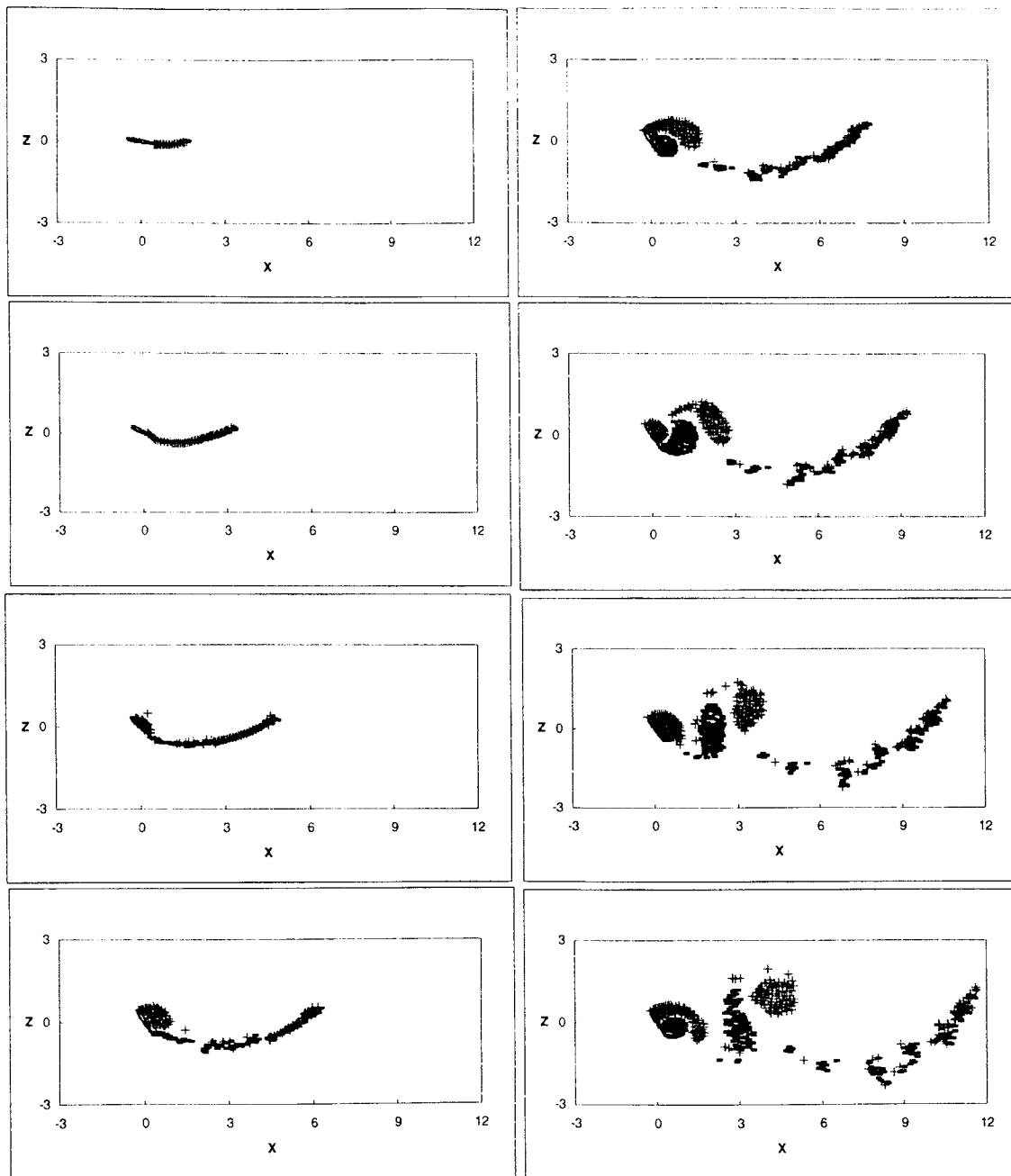
Figure 32. Wake picture for pitch ($\alpha_{nd} = 0.02$) and hold case.

The separation transition modelling is at the core of the accuracy limitations of the present model. A separation location predictor like that given in Stratford[32], to actually model the transition of the boundary layer separation, might be a benefit. Although difficulties might then arise in its extension to a fully unsteady simulation.

Analyzing the separation transition process, by modifying the parameters in equation 19, is necessary to understand the cause and effect of these changes on the lift. Test cases for parameter changes of equation 19 are shown in Figure 33. All cases here represent an α_{nd}=0.036 to show an example of the relative effects of the parameter changes on $C_{l\alpha}$ compared to those obtained from Jumper.[27] The test uses an 80 panel NACA 0015 airfoil with an initial upper separation panel number of 68. τ_2 is held constant at 0.85 while τ_1 is adjusted. Also shown in Figure 33 is the corresponding effect these parameter changes had on the separation panel location as a function of angle of attack. As can be seen, the effect of increasing τ_1 is to delay the transition of the separation location as expected, as well as delaying the lift coefficient fall off. What is also interesting to note is the plateauing effect this parameter change induces. As τ_1 is increased, the slope of the lift curve when separation point transition is occurring, and slightly thereafter, shifts from a positive slope to a slightly negative slope. This can also be attributed to the speed with which transition occurs. The delay to leading edge stall serves as a means with which the large leading edge separation vortex can remain closer to the airfoil for a longer time span, thereby affecting the pressures in that vicinity.

CHAPTER IV

CONCLUSIONS AND RECOMMENDATIONS

4.1 Conclusions

The goal of the current study was to develop a simplified model for the unsteady separated flow field on airfoils in stall which captured the primary flow physics. The model was applied to relevant physical configurations in the stall regime and qualitatively captured all of the loading behavior of the two dimensional vehicle, unsteady flow field behavior, and unsteady pressure effects. The computational results have also led to the conclusion that certain complex aerodynamic problems may be governed primarily by unsteady inviscid phenomena. While other techniques such as full solution of the unsteady Navier-Stokes equations may provide a better quantitative match with experiment, the fundamentals of the problem may be hidden within the added complexity. The model also provided a faster, more efficient computational model when compared to the time required to run Navier-Stokes based codes when detailed analysis of the entire flowfield is not required.

The attached flow analysis indicate that the computational model quantitatively captured the dominant features of the flowfield observed in experiment as well as those results obtained from theoretical solutions. These include lift and moment coefficients, wake characteristics, and pressure coefficients.

Furthermore, the separated model accurately duplicated the time averaged lift and moment compared with experiment. The separation model also demonstrated the

separated wake's alternate wake shedding effect on a tandem airfoil configuration and the resulting dynamic changes to the total lift and moment. Finally, the model qualitatively described the effects of dynamic stall on an airfoil pitching at a constant rate.

There are, however, some limitations to the separation model. It was shown that the separation point transition process is sensitive to parameter changes. Although the model qualitatively captured the dynamic stall effects, i.e. the delay in lift coefficient fall off due to an increased rate of change of angle of attack, the model, at present, did not fully capture the magnitudes of the experimental results. However, the error may also be due to factors pertaining to the experimental test setup, for example, surface roughness of the airfoil, the wake's diffusion aft of the test section, turbulence intensity, ensemble averaging of the collected data, as well as three dimensional effects. Furthermore, the qualitative success of the simple state-variable approach for modelling the separation process provides a basis from which further research can be done. Also, the manner of determining the parameters that best meet experimental results can be considered a calibration process. One should keep in mind that each airfoil tested has its own unique characteristics thereby adding uniqueness to the experimental test as well as having its own unique parameters.

4.2 Recommendations

The computational model does provide a means by which complicated separated flows may be analyzed in an efficient manner. The possibilities for the direction of further developments and enhancements of the code are endless. They include adding motion, by coupling of the flowfield solution with the rigid body equations of motion, to the tandem airfoil configuration to study the dynamic interactions between the two moving bodies, including aeroelastic motion by adding spring models to simulate structural forces, analyzing longitudinal dynamic stability in stall, continued

experimentation with the state variable separation model to better simulate the experimental dynamic stall data, possibly including an unsteady separation predictor rather than the state space representation, as well as including a post processor for in the loop animation of the flowfield in real time.

BIBLIOGRAPHY

1. Clements, R.R., Maull, D.J., "The representation of sheets of vorticity by discrete vortices," Prog. Aerospace Sci., Vol. 16, pp. 129-146, 1975

2. Sarpkaya, T., "Computational Methods with Vortices-the 1988 Freeman Scholar Lecture," J. Fluids Engineering, Vol. 111, March 1989.

3. Von Karman, T., Sears, W.R., "Airfoil Theory for Non-Uniform Motion," J. of the Aeronautical Sciences, Vol. 5, No. 10, 1938

4. Theordesen, T., "General Theory of Aerodynamic Instability and the Mechanism of Flutter," NACA TR 496, 1935.

5. Wagner, H., "Dynamischer Auftrieb von Tragflügeln," Zeilschrift fuer Angewandte Mathematik und Mechanik, Vol. 5, p. 17, 1925.

6. Küssner, H.G., "Das zweidimensionale Problem der beliebig bewegten Tragfläche unter Berücksichtigung von Partialbewegungen der Flüssigkeit," Luftfahrtforschung, Vol 17, 1940, p. 355.

7. Küssner, H.G., Gorup, G.V., "Instationäre linearisierte Theorie der Flügelprofile endlicher Dicke in kompressibler Strömung," Mitteilungen des Max-Planck-Instituts für Strömungssorschung und der Aerodynamischen Versuchsanstalt, No. 26, Göttengin, 1960.

8. Van De Vooren, A.I., Van De Vel, H.,"Unsteady Profile Theory in Incompressible Flow," Archiwum Mechanik Stosowanej, Vol. 3, No. 16, 1964.

9. Hewson-Browne, R.C., "The Oscillation of a Thick Airfoil in an Incompressible Flow," Mechanics and Applied Mathematics, Vol. XVI, Feb. 1963.

10. Basu, B.C., Hancock, G.J., "The Unsteady Motion of a Two-dimensional Aerofoil in Incompressible Inviscid Flow," J. Fluid Mech., Vol. 87, part 1, pp. 159-178, 1978.

11. Hess, J.L., Smith, A.M.O., "Calculation of Potential Flow About Arbitrary Bodies." Prog. Aero. Sci., Vol. 8, No. 1, 1967.

12. Giesing, J.P., "Vorticity and Kutta Condition for Unsteady Multienergy Flows'," Transactions of the ASME, pp. 608-613, Sept. 1969.

13. Sears, W. R., "Unsteady Motion of Airfoils with Boundary Layer Separation," AIAA Journal, Vol 14, No. 2, pp. 216-220, 1976.

14. Sarpkaya, T., "An Inviscid Model of Two-dimensional Vortex Shedding for Transient and Asymptotically Steady Separated Flow Over an Inclined Plate," J. Fluid Mech., Vol. 46, pp. 241-258, 1975.

15. Kiya, M., Arie, M., "A Contribution to an Inviscid Vortex Shedding Model for an Inclined Flat Plate in Uniform Flow," J. Fluid Mech., Vol. 82, pp. 223-240, 1977.

16. Methta, B.U., "Dynamic Stall of an OscillatingAirfoil," AGARD Fluid DynamicsPanel Symp. on Unsteady Aerodynamics," Ottawa, Canada, Paper 22, 1977.

17. Katz, J., "A Discrete Vortex Method for the Non-steady Separated Flow Over an Airfoil," J. Fluid Mech., Vol. 102, part 1, pp. 315-328, 1981.

18. Fage, A., Johansen, F.C., "On the Flow of Air Behind an Incined Flat Plate of Infinite Span," Proc. Roy. Soc., A 116, pp. 170-197, 1927

19. Arena, A. S., Nelson, R.C., "A Discrete Vortex Model for Predicting Wing Rock of Slender Wings," AIAA, 92-4487, 1992.

20. Huyer, S.A., Grant, J.R., Uhlman, J.S., "A Vortex Element Representation of Two-Dimensional Unsteady Flow Fields," AIAA, 94-0075, 1994.

21. Chorin, A.J.,"Numerical Study of Slightly Viscous Flow," J. Fluid Mech., Vol. 57, pp. 785-796, 1973.

22. Chow, C., *An Introduction to Computational Fluid Mechanics*, Seminole Publishing, Boulder, CO.,1983.

23. Prandtl, L., "Über Flüssigtkeitsbewegung bei sehr kleiner Reibung," Proc. III Intern. Math. Congr., Heidelberg, 1904

24. Giesing, J.P., "Nonlinear Two Dimensional Unsteady Potential Flow with Lift," J. Aircraft 1968, Vol. 5, No. 4.

25. Katz, J., Plotkin, A., *Low-speed Aerodynamics*, McGraw-Hill, Inc., 1991.

26. Mendenhall, M. et al., *Tactical Missile Aerodynamics: Prediction Methodology*, Vol. 142, AIAA, 1992.

27. Jumper, E.J., Dimmick, R.L., Allaire, A.J.S., "The Effect of Pitch Location on Dynamic Stall," ASME, Forum on Unsteady Flow Separation, Vol. 52, pp. 201-220, 1988

28. Goman, M., Khrabrov, A., "State Space Representation of Aerodynamic Characteristics of an Aircraft at High Angles of Attack," AIAA, 92-4651-CP, pp. 759-766, 1992.

29. Critzos, C.C., "Aerodynamic Characteristics of NACA 0012 Airfoil Section at Angles of Attack from 0° to 180°," NACA TN 3361, 1956

30. Stengel, R.F., "Stalling Characteristics of a General Aviation Aircraft," J. Aircraft, Vol. 19, No. 6, pp. 425-433, 1982

31. Helin, H.E., "Experimental Studies on the Dynamic Development and Control of Unsteady Separated Flows," Doctoral Thesis, University of Colorado, Boulder, CO, 1986.

32. Stratford, B.S., "The Prediction of Separation of the Turbulent Boundary Layer," J. Fluid Mech., Vol. 5, pp. 1-16, 1959.

APPENDIX

```
c234567890123456789012345678901234567890123456789012345678901234567890123456789012
*                                                                                *
*         program wingsep                                                        *
*                                                                                *
*         written by:    Todd Perfito      Aero/Mech Engimeering                 *
*                        May, 1994         Oklahoma State University             *
*                                                                                *
*                                                                                *
*         This program calculates the aerodynamic solution for an                *
*         arbitrary airfoil in arbirary motion, to include dynamic stall,        *
*         and the resulting unsteady velocities, pressures, and loading.         *
*                                                                                *
*********************************************************************************
*                                                                                *
*         variable definition                                                    *
*                                                                                *
*         inputs:                                                                *
*                                                                                *
*         m       .......   panel number                                         *
*         alphad  .......   angle of attack (deg)                                *
*         itot    .......   total step count                                     *
*         dt      .......   time step                                            *
*         nsep    .......   initial panel number for upper separation pt.        *
*         tau1    .......   delay in sep.'s initial startup compared w/ss        *
*         tau2    .......   delay in sep.'s transition to le compared w/ss       *
*         msep    .......   number of total separation pts. (1 or 2)             *
*         npit    .......   is there motion? (1-yes)                             *
*         xcg     .......   center of rotation and moment                        *
*         nmotn   .......   type of motion: pitch, plunge, or aeroelas.          *
*         adot    .......   ramp nondimensional pitch rate                       *
*         delay   .......   ramp motion delay in startup (itot*dt)               *
*         stop    .......   ramp motion stop (nondimen sec. (itot*dt)            *
*         freq    .......   oscillation frequency                                *
*         amp     .......   max pitch aoa in oscill.                             *
*         h0      .......   max plunge height (h/c)                              *
*         phih    .......   phase shift of plunge to pitch                       *
*                                                                                *
*           Under experiment and validation for aeroelasticity                   *
*         ratio   ...... :.reduced bending/torsion frq. ratio                    *
*         mstar   ...... :.reduced density ratio                                 *
*         xalph   ...... :.dimensionless static unbalance                        *
*         ralphsq...... :.dimensionless radius of gyration^2                     *
*                        :                                                        *
*                   refer bisplinghoff "aeroelasticity"                          *
*                                                                                *
*  =============================================================================  *
*                                                                                *
*         [matrices]:                                                            *
*                                                                                *
*         ep      .......   loc. of panel endpts converted to clockwise          *
*         ept     .......   loc. of panel endpts f/ subrtn body (pnl gen.)       *
*         pt1     .......   loc. of 1st panel endpoint for all panels            *
*         pt2     .......   loc. of 2nd panel endpoint for all panels            *
*         pi      .......   pi                                                    *
*         co      .......   loc. of panel colocation points                      *
*         a       .......   normal influence coefficients                        *
*         b       .......   tangent influence coefficients                       *
*         g       .......   solution vector                                      *
*         aa      .......   influence coefficients storage                       *
*         th      .......   angles between local pnl coord. sys. to global       *
*         dl      .......   panel lengths                                        *
*         vposi   .......   initial nascent vortices positions                   *
*         vpos    .......   vortex positions                                     *
*         vtemp   .......   iterated vortex positions                            *
*         vposo   .......   old vortex positions                                 *
```

```
*       vpost   .......  new vortex positions                      *
*       gam     .......  vortex strengths                          *
*       angl    .......  nascent vortex rel. chng in postn wrt col. pts *
*       cpq     .......  pressure coefficients due to steady flow  *
*       cpbf    .......  pressure coefficients due to airfoil motion *
*       cpdphi .......  pressure coefficients due to unsteady flow *
*       phil    .......  previous potential strengths at each panel *
*       dphil   .......  change in potential strengths at each panel *
*       dphil2 .......  "                                        " *
*       dphil3 .......  "                                        " *
*       wupstr .......  w-velocities alng line nrml to lwr srfc mdpnl *
*       cp      .......  pressure coefficients                     *
*       ej      .......  wing position for other animation         *
*                                                                  *
* ================================================================ *
*                                                                  *
*       scalars:                                                   *
*                                                                  *
*       ac      .......  aerodynamic center                        *
*       nanimt .......  flag write animation file (y/n)            *
*       nskip   .......  number of animation frames to skip        *
*       dti     .......  nascent vortex position iteration multiplier *
*       crf     .......  circulation reduction factor (always 1.0) *
*       core    .......  discrete vortex core model diameter (dt)  *
*       gamwk   .......  total vorticity sum of wake strengths     *
*       itime   .......  total step counter                        *
*       itcount.......  total iteration counter                    *
*       xsepl   .......  last position of sep pt                    *
*       nqt     .......  animation flag for mac quicktime          *
*                                                                  *
* ================================================================ *
*                                                                  *
*       subroutines:                                               *
*                                                                  *
*       xzvel   .......  calculates the induced velocity at any point *
*                        due to flagged singularities in global (body *
*                        fixed) coordinates                        *
*                                                                  *
*       body    .......  calculates endpoints of any 4-digit naca  *
*                        series airfoil                            *
*                                                                  *
*       matrx   .......  gaussian elimination matrix solver (a-matrix *
*                        destroyed at every solution               *
*                                                                  *
************************************************************************

        character*8 title(10)
        character*12 namelift,nameanim,namein

        real ep(100,2), ept(100,2), pt1(100,2), pt2(100,2), pi
        real co(100,2), a(100,100), b(100,100), g(100), aa(100,100)
        real th(100), dl(100), vposi(2,2), vpos(2,2,500), vtemp(2,2)
        real vposo(2,2), vpost(2,2,500), gam(2,500), angl(2,4)
        real cpq(100), cpbf(100), cpdphi(100), mstar
        real phil(100), dphil(100), dphil2(100), dphil3(100)
        real wupstr(101), cp(100), ej(100,2)

        pi=4.*atan(1.)
        xcg=0.
        i1=0

        title(1)='cox'
        title(2)='cp'
        title(3)='epx'
        title(4)='epz'
```

```fortran
      title(5)='vpos1x'
      title(6)='vpos1z'
      title(7)='vpos2x'
      title(8)='vpos2z'

      write(*,*)'enter output loads file name '
      read(*,'(a)')namelift
      write(*,*)'enter output animation file name '
      read(*,'(a)')nameanim
      write(*,*)'enter input file name '
      read(*,'(a)')namein

      open(10,file=nameanim)
      open(11,file=namelift)
      open(12,file=namein)

      read (12,*) m,alphad,itot,dt,nsep,tau1,tau2,msep,npit,xcg,nmotn
     & ,adot,delay,stop,freq,amp,h0,phih,ratio,mstar,xalph,ralphsq

      phih=phih*pi/180.
      adot=adot*2.
      freq=2.*freq
      if(ratio.eq.0.) then
       wh=0.
       wa=0.
      else
       wh=1./ratio
       wh=wh*ratio
       wa=wh*ratio
      end if
      omeg=0.
      hdot=0.

      write (11,*)'time,alpha,cl,cmc/4,cd'

      ac=xcg
      nanimt=1
      n = m + 1 + nsep

      if (itot.le.100) then
       nskip = 1.
      else
       nskip = itot/100
      end if
      write(10,*)itot,',',dt,',',nskip,',',xcg

      alpha = alphad*pi/180.
      alphao= alpha

      dti=dt/1000.

      crf = 1.
      core = dt
      gamwk = 0.
      itime = 0
      itcount = 1
      omeg = 0.
      xsepl = 1.-xcg
      nqt = 0

1     continue

c     initialize matrices
      do i=1,n+1
        do j=1,n+1
```

```
        a(i,j)=0.0
          end do
c           phil(i)=0.0
        end do

        do i=1,1000
          do j=1,2
            gam(j,i)=0.
        end do
        end do

c      read in the panel end points

          call body(m,ept,xcg)

c      convert panelling to clockwise

        do i=1,m+1
          ep(i,1)=ept(m+1-i+1,1)
          ep(i,2)=ept(m+1-i+1,2)
        end do

c      establish coordinates of panel end points

        do i=1,m
          pt1(i,1)=ep(i,1)
          pt2(i,1)=ep(i+1,1)
          pt1(i,2)=ep(i,2)
          pt2(i,2)=ep(i+1,2)
        end do

c      find panel angles th(j) and length

        tlength = 0.

        do i=1,m
          dz=pt2(i,2)-pt1(i,2)
          dx=pt2(i,1)-pt1(i,1)
          th(i)=atan2(dz,dx)
          dl(i) = sqrt(dx**2+dz**2)
         tlength = tlength + dl(i)
        end do

c      establish colocation points

        do i=1,m
            co(i,1) = (pt2(i,1)-pt1(i,1))/2+pt1(i,1)
            co(i,2) = (pt2(i,2)-pt1(i,2))/2+pt1(i,2)
          end do

        vposi(1,1)= ep(1,1) + 0.01
        vposi(1,2)= ep(1,2) + 0.

        write(*,*)co(ms,1),co(ms,2)
c===============================================================================

  5     continue
          itime = itime + 1
          itcount = 1
          time = itime*dt


c                            pitching & plunging motion

        if(npit.eq.1.and.nmotn.eq.1.and.time.ge.delay.and.
```

65

```
    & time.lt.stop) then
        omeg = adot
        alpha = alphao + adot*(time-delay)
        alphad = alpha*180./pi
      else if(npit.eq.1.and.nmotn.eq.1.and.time.ge.stop) then
        omeg=0.
      else if(npit.eq.1.and.nmotn.eq.2) then
        omeg = amp*pi/180.*freq*cos(freq*time)
        alpha = alphao + amp*pi/180.*sin(freq*time)
        alphad = alpha*180./pi
        h = h0*sin(freq*time-phih)
        hdot = h0*freq*cos(freq*time-phih)
      else if(npit.eq.1.and.nmotn.eq.3) then
        alphal=alpha
        omegl=omeg
        hdotl=hdot
        hl=h

        omeg=(-2.*wh**2*xalph*hl+ralphsq*wa**2*alphal-(4.*clt*xlaph
     &       +8.*cm)/(pi*mstar))*dt/(xalph**2-ralphsq) + omegl
        alpha=omegl*dt + alphal
        alphad = alpha*180./pi
        hdot=(ralphsq*wh**2*hl-ralphsq*wa**2*xalph*alphal/2.+(4.*cm*xalph
     &       +2.*clt*ralphsq)/(pi*mstar))*dt/(xalph**2-ralphsq) + hdotl
        h=hdotl*dt + hl
      end if

c
c                                 separation criteria
c

      if (nsep.eq.2)then

        xo = 1.-xcg
        sepdel = alphad - tau2*omeg*180./pi
        if (sepdel.gt.14.) then
         if (sepdel.lt.20.)xo=(-.17041+.00673*sepdel)/(1.-.07701*sepdel)
     &                         -xcg
         if (sepdel.ge.20.)xo=.05-xcg
        end if
        xsep = xsepl + (xo-xsepl)*dt/tau1
        xsepl= xsep

        if (xsep.ge.(1.-xcg)) xsep = co((m-3),1)
        do i=m/2,m
         if (pt1(i,1).lt.xsep.and.pt2(i,1).gt.xsep) then
           ms = i
           if(ms.ge.msep)ms=msep
           if(ms.eq.msep.and.alphad.lt.0.) ms=m-msep
           xsep = co(ms,1)
           zsep = co(ms,2)
           vposi(2,1) = co(ms,1) - dl(i)*sin(th(ms))/2.
           vposi(2,2) = co(ms,2) + dl(i)*cos(th(ms))/2.
           go to 7
         end if
        end do
      end if

7       do i=1,nsep
         x=vposi(i,1)*cos(alpha)+vposi(i,2)*sin(alpha)+h*sin(alpha)
         z=vposi(i,2)*cos(alpha)-vposi(i,1)*sin(alpha)-h*cos(alpha)
         vpos(i,1,itime)=x
         vpos(i,2,itime)=z
        end do
10      continue
```

```fortran
      if (itime.eq.1.and.itcount.eq.1) then

c     establish influence coefficients

      do i=1,m
        uv=0.
        wv=0.
        do j=1,m

c     convert colocation point to local panel coordinates
        xt=co(i,1)-pt1(j,1)
        zt=co(i,2)-pt1(j,2)
        x2t=pt2(j,1)-pt1(j,1)
        z2t=pt2(j,2)-pt1(j,2)

        x=xt*cos(th(j))+zt*sin(th(j))
        z=-xt*sin(th(j))+zt*cos(th(j))
        x2=x2t*cos(th(j))+z2t*sin(th(j))
        z2=0.

c     find r1, r2, th1, th2
        r1=sqrt(x**2+z**2)
        r2=sqrt((x-x2)**2+z**2)

        th1=atan2(z,x)
        th2=atan2(z,x-x2)

c     compute velocity in local reference frame

        if(i.eq.j) then
          ul=0.
          wl=0.5
          ulv= 0.5
          wlv= 0.
        else
          ul=1./(2.*pi)*log(r1/r2)
          wl=1./(2.*pi)*(th2-th1)
          ulv = 1./(2.*pi)*(th2-th1)
          wlv = 1./(2.*pi)*log(r2/r1)
        end if

c        return velocity to global reference frame

        u=ul*cos(-th(j))+wl*sin(-th(j))
        w=-ul*sin(-th(j))+wl*cos(-th(j))
        uv = uv + ulv*cos(-th(j)) + wlv*sin(-th(j))
        wv = wv - ulv*sin(-th(j)) + wlv*cos(-th(j))


c        a(i,j) is the influence coefficient defined by the
c        tangency condition.  b(i,j) is the induced local
c        tangential velocity to be used in cp calculation

        a(i,j)=-u*sin(th(i))+w*cos(th(i))
        b(i,j)=u*cos(th(i))+w*sin(th(i))

          end do

        a(i,m+1) = -uv*sin(th(i)) + wv*cos(th(i))
          b(i,m+1) = uv*cos(th(i)) + wv*sin(th(i))

          end do

          do k=1,m
```

```fortran
        do l=1,m+1
          aa(k,l) = a(k,l)
        end do
      end do

    end if

  do i=1,m
    uv = 0.
    wv = 0.
    do j=1,m+1
      a(i,j) = aa(i,j)
    end do
```

```fortran
c      shed vortex influence

    x = vpos(1,1,itime)*cos(alpha) - vpos(1,2,itime)*sin(alpha)
    z = vpos(1,2,itime)*cos(alpha) + vpos(1,1,itime)*sin(alpha)+h
    xright = co(i,1) - x
    zright = co(i,2) - z
    uright = 1./(2.*pi)*zright/(xright**2+zright**2)
    wright = -1./(2.*pi)*xright/(xright**2+zright**2)

    a(i,m+2) = -uright*sin(th(i)) + wright*cos(th(i))
    aa(i,m+2) = a(i,m+2)
    b(i,m+2) = uright*cos(th(i)) + wright*sin(th(i))

    if (nsep.eq.2) then
      x = vpos(2,1,itime)*cos(alpha) - vpos(2,2,itime)*sin(alpha)
      z = vpos(2,2,itime)*cos(alpha) + vpos(2,1,itime)*sin(alpha)+h
      xleft = co(i,1) - x
      zleft = co(i,2) - z
      uleft = 1./(2.*pi)*zleft/(xleft**2+zleft**2)
      wleft = -1./(2.*pi)*xleft/(xleft**2+zleft**2)

      a(i,m+3) = -uleft*sin(th(i)) + wleft*cos(th(i))
      aa(i,m+3) = a(i,m+3)
      b(i,m+3) = uleft*cos(th(i)) + wleft*sin(th(i))
    end if
```

```fortran
c      rhs

    dx = co(i,1)
    dz = co(i,2)
    call xzvel(u,w,co(i,1),co(i,2),alpha,pt1,pt2,g,th,m
 &   ,vpos,gam,itime,0,0,0,0,nsep,core,h)
    a(i,n+1)=(cos(alpha)-hdot*sin(alpha)-omeg*dz)*sin(th(i))
 &          -(sin(alpha)+hdot*cos(alpha)+omeg*dx)*cos(th(i))
 &          + u*sin(th(i)) - w*cos(th(i))
    aa(i,n+1) = a(i,n+1)

  end do
```

```fortran
c    kutta condition

    do j=1,n
      a(m+2,j) = 0.
      aa(m+2,j) = a(m+2,j)
      a(m+1,j) = b(1,j) + b(m,j)
      aa(m+1,j) = a(m+1,j)
      if (nsep.eq.2) then
        a(m+3,j) = b(ms,j)
        aa(m+3,j) = a(m+3,j)
      end if
    end do
```

```fortran
      call xzvel(u,w,co(1,1),co(1,2),alpha,pt1,pt2,g,th,m
     & ,vpos,gam,itime,0,0,0,0,nsep,core,h)
          uk1 = u
          wk1 = w
      call xzvel(u,w,co(m,1),co(m,2),alpha,pt1,pt2,g,th,m
     & ,vpos,gam,itime,0,0,0,0,nsep,core,h)
          ukm = u
          wkm = w

          a(m+1,n+1) = - ( cos(alpha-th(1)) + cos(alpha-th(m)) )
     &       - ( uk1*cos(th(1)) + wk1*sin(th(1)) )
     &    - ( ukm*cos(th(m)) + wkm*sin(th(m)) )
          aa(m+1,n+1) = a(m+1,n+1)

          if (nsep.eq.2) then

      call xzvel(u,w,co(ms,1),co(ms,2),alpha,pt1,pt2,g,th,m
     & ,vpos,gam,itime,0,0,0,0,nsep,core,h)
          a(m+3,n+1) = - ( cos(alpha-th(ms)) )
     &    - (u*cos(th(ms)) + w*sin(th(ms)) )
          aa(m+3,n+1) = a(m+3,n+1)
          end if


c     kelvin condition

          a(m+2,m+1) = tlength
          aa(m+2,m+1) = a(m+2,m+1)
          a(m+2,m+2) = 1.
          aa(m+2,m+2) = a(m+2,m+2)
          if (nsep.eq.2) then
           a(m+2,m+3) = crf
           aa(m+2,m+3) = a(m+2,m+3)
          end if
          a(m+2,n+1) = - gamwk
          aa(m+2,n+1) = a(m+2,n+1)


c     solve for solution vector

      n=n+1
      call matrx(a,n,g)
      n=m+1+nsep

      do i=1,nsep
      gam(i,itime) = g(m+1+i)
      end do

      do i=1,nsep
       x = vpos(i,1,itime)*cos(alpha) - vpos(i,2,itime)*sin(alpha)
       z = vpos(i,2,itime)*cos(alpha) + vpos(i,1,itime)*sin(alpha)+h
       call xzvel(u,w,x,z,alpha,
     & pt1,pt2,g,th,m,vpos,gam,itime,0,1,1,1,nsep,core,h)

       vtemp(i,1) = vposi(i,1)+u*dti
       vtemp(i,2) = vposi(i,2)+w*dti

       angl(i,1) = angl(i,2)
       angl(i,2) = angl(i,3)
       angl(i,3) = angl(i,4)
       angl(i,2) = atan2(w,u)
       if(mod(itime,10).eq.0)write(*,*)i,'angl=',angl(i,2)*180./pi
      end do

      do i=1,nsep
```

```fortran
        x=vtemp(i,1)*cos(alpha)+vtemp(i,2)*sin(alpha)+h*sin(alpha)
        z=vtemp(i,2)*cos(alpha)-vtemp(i,1)*sin(alpha)-h*cos(alpha)
        vpos(i,1,itime) = x
        vpos(i,2,itime) = z
      end do

      itcount = itcount + 1

      tnorm = sqrt((angl(1,2) - angl(1,1))**2)/sqrt(angl(1,2)**2)

      if (itcount.eq.40) then
       write (*,*) 'too many steps, taking last iterated position'
        tnorm=0.
      end if
      if(tnorm.gt.1e-6)goto 10


c     convect wake in time

      do i=1,itime
         do j=1,nsep

           x = vpos(j,1,i)*cos(alpha) - vpos(j,2,i)*sin(alpha)
           z = vpos(j,2,i)*cos(alpha) + vpos(j,1,i)*sin(alpha)+h
           call xzvel(u,w,x,z,alpha
     &         ,pt1,pt2,g,th,m,vpos,gam,itime,i1,1,1,1,nsep,core,h)
           if(i1.ne.0) then
             utemp=u*cos(th(i1))+w*sin(th(i1))
             wtemp=-u*sin(th(i1))+w*cos(th(i1))
             if(wtemp.lt.0.) wtemp=0.
             u=utemp*cos(th(i1))-wtemp*sin(th(i1))
             w=utemp*sin(th(i1))+wtemp*cos(th(i1))
           end if
           uiner = u*cos(alpha) + w*sin(alpha)
           winer = w*cos(alpha) - u*sin(alpha)
           vpost(j,1,i) = vpos(j,1,i) + uiner*dt
           vpost(j,2,i) = vpos(j,2,i) + winer*dt
         end do
      end do

      tgam = g(m+1)*tlength + gamwk + g(m+2) + g(m+3)*crf

      gamwk = 0.
      do i=1,itime
         do j=1,nsep
            gamwk = gamwk + gam(j,i)
         end do
      end do

c     convert source strengths into tangential velocities
c     along the airfoil surface and cp's on each panel

      d1 = gam(2,itime)/dt
      d2 = gam(2,itime-1)/dt
      d3 = gam(2,itime-2)/dt
      d4 = gam(2,itime-3)/dt
      clqt = 0.
      clbft = 0.
      cldphit = 0.
      phi=0.
      cm = 0.
      cd=0.
     do i=1,m
      vel=0.
      veln=0.
```

```fortran
       dx = co(i,1)
       dz = co(i,2)
      do j=1,n
       vel = vel + b(i,j)*g(j)
       veln= veln + aa(i,j)*g(j)
      end do
      call xzvel(u,w,co(i,1),co(i,2),alpha,pt1,pt2,g,th,m,vpos
     &          ,gam,itime,0,0,0,0,nsep,core,h)

      vwake = u*cos(th(i)) + w*sin(th(i))
      vwaken= -u*sin(th(i)) + w*cos(th(i))

      qt = vel + vwake
      qn = veln + vwaken

      if(i.eq.m/4) qz=qn*cos(th(i))+qt*sin(th(i))

      bftran = (cos(alpha)+omeg*dz)*(qt*cos(th(i))-qn*sin(th(i)))
     &          +(sin(alpha)+hdot-omeg*dx)*(qt*sin(th(i))+qn*cos(th(i)))

      phi = phi + qt*dl(i)
      dphi=(phi-phil(i))/dt

      if (i.ge.ms.and.nsep.eq.2) then
c        avgdphi=(dphi+dphil(i)+dphil2(i)+dphil3(i)+d1+d2+d3+d4)/4.
       avgdphi=dphi+d1
      else
       avgdphi=dphi
      end if

      cpq(i) = - qt**2 - qn**2
      cpbf(i) = -2.*bftran
      cpdphi(i) = -2.*(avgdphi)

      clqt = clqt - cpq(i)*dl(i)*cos(th(i)-alpha)
      clbft = clbft - cpbf(i)*dl(i)*cos(th(i)-alpha)
      cldphit = cldphit - cpdphi(i)*dl(i)*cos(th(i)-alpha)
      cd=cd-(cpq(i)+cpbf(i)+cpdphi(i))*dl(i)*sin(alpha-th(i))
      cm=cm+(cpq(i)+cpbf(i)+cpdphi(i))*dl(i)*
     &      (cos(th(i))*(co(i,1)+xcg-ac) + sin(th(i))*co(i,2))

      dphil3(i)=dphil2(i)
      dphil2(i)=dphil(i)
      dphil(i)=dphi
      phil(i)=phi
      end do
     clt = clqt + clbft + cldphit
     write(11,50)time,alphad,clt,cm,cd

c                   upstream potential

     do i=101,2,-1
      z=.1-i*.1
      if(z.gt.co(m/4,2)) go to 45
      x=co(m/4,1)
      call xzvel(u,w,x,z,alpha,pt1,pt2,g,th,m,vpos
     &          ,gam,itime,0,0,1,1,nsep,core,h)
      wupstr(i)=w
     end do

45   phiupsl=phiups
     phiups=0.
     do j=101,i+2,-1
      phiups=phiups+.1*(wupstr(j)+wupstr(j-1))/2.
     end do
```

71

```fortran
      phiups=phiups+((i+1)*.1-co(m/4,2))*(wupstr(i+1)+qz)/2.

      do i=1,m
       cp(i)=cpq(i)+cpbf(i)+cpdphi(i)-2.*(phiups-phiupsl)/dt
      end do



      do i=1,41
      ej(i,1)=ep(i,1)*cos(alpha)+ep(i,2)*sin(alpha)+h*sin(alpha)
      ej(i,2)=ep(i,2)*cos(alpha)-ep(i,1)*sin(alpha)-h*cos(alpha)
      end do

      if (mod(itime,nskip).eq.0.and.nqt.eq.1) then
       write (13,55) title(1),(co(i,1),i=1,40)
       write (13,55) title(2),(cp(i),i=1,40)
       write (13,56) title(3),(ej(i,1),i=1,41)
       write (13,56) title(4),(ej(i,2),i=1,41)
       write (13,57) title(5),(vpos(1,1,i),i=1,itime)
       write (13,57) title(6),(vpos(1,2,i),i=1,itime)
       write (13,57) title(7),(gam(1,i),i=1,itime)
       if(nsep.eq.2)write (13,57) title(8),(vpos(2,1,i),i=1,itime)
       if(nsep.eq.2)write (13,57) title(9),(vpos(2,2,i),i=1,itime)
       if(nsep.eq.2)write (13,57) title(10),(gam(2,i),i=1,itime)
      end if

        if(nanimt.eq.1.and.mod(itime,nskip).eq.0) then
         write(10,*) itime*dt,alpha,h
         do i=nskip,itime,nskip
          write(10,*)vpos(1,1,i),',',vpos(1,2,i),',',gam(1,i)
         end do
         do i=nskip,itime,nskip
          write(10,*)vpos(2,1,i),',',vpos(2,2,i),',',gam(2,i)
         end do
        end if


        do i=1,itime
            do j=1,nsep
             vpos(j,1,i) = vpost(j,1,i)
             vpos(j,2,i) = vpost(j,2,i)
            end do
        end do


        if(mod(itime,10).eq.0) write(*,*)itime,tgam,alphad,ms
        if(itime.lt.itot)goto 5


50    format (8(f12.5,','),f12.5)
51    format (i4,',',3(f12.5,','),f12.5)

55    format (a,',',39(f12.5,','),f12.5)
56    format (a,',',40(f12.5,','),f12.5)
57    format (a,',',499(f12.5,','),f12.5)


      stop
      end


c=====================================================================

      subroutine matrx(a,n,g)
```

```
c              matrx is a matrix reducer of the gaussian type
c              a(i,j) is the matrix, g(i) is the solution vector

        real a(100,100),temp(100,100),g(100)


c              initialize the g vector to all zeros

      do i=1,n-1
       g(i)=0.
      end do

c              convert coefficient matrix
c              to upper triangular form

      do i=1,n-1
 5     if(abs(a(i,i)).lt.0.0000001)goto 9

      p=a(i,i)
      do j=i,n
       a(i,j)=a(i,j)/p
      end do

      do k=i+1,n-1
       p2=a(k,i)
        do l=i,n
         a(k,l)=a(k,l)-p2*a(i,l)
        end do
      end do
      end do

c              back substitute triangularized matrix to get
c              values of solution vector

      do i=n-1,1,-1
       g(i)=a(i,n)
        do j=1,n-1
         a(i,i)=0.
         g(i)=g(i)-a(i,j)*g(j)
        end do
      end do

      return

c              order matrix so that diagonal coefficients are
c              not=0 and stop if matrix is singular

 9     if(i.ne.n-1)then
       do j=1,n
        temp(i,j)=a(i,j)
        a(i,j)=a(i+1,j)
        a(i+1,j)=temp(i,j)
       end do
       goto 5
      else
       goto 10
      end if

 10    write(*,*)' no solution '

      stop
      end

c=======================================================================
```

73

```fortran
      subroutine body(m,ept,xcg)

c          this subroutine calculates the nodal coordinates
c          of the body surface panels
c     ***  note: panel 1 @ te. top sfc., numbering scheme
c                counter-clockwise                    ***

      real pi,theta,xc,thick,z,ept(100,2)

      pi=4.*atan(1.)

      do i=1,m+1
        theta=2.*pi*float(i-1)/float(m)
          xc =  ( 1. + cos(theta) )/2.
        thick = 1.2*(0.2969*sqrt(xc)-0.126*xc-.3537*xc**2
     & + .2843*xc**3 - .1015*xc**4)
       z = thick*sign(1.,sin(theta))/2.
          ept(i,1)=xc-xcg
      ept(i,2)=z
      end do

      return
      end

c=====================================================================

      subroutine xzvel(u,w,x,z,alpha,pt1,pt2,g,th,m,vposo,gam,
     & itime,i1,i2,i3,i4,nsep,core,h)

      real pi,x,z,alpha,g(100),th(100),vposo(2,2,500),pt1(100,2)
      real pt2(100,2),gam(2,500),r

      pi=4.*atan(1.)
c     wing influence

      uwing=0.
      wwing=0.

         if(i3.eq.1)then
        i1=0
      do j=1,m

      xt=x-pt1(j,1)
      zt=z-pt1(j,2)
      x2t=pt2(j,1)-pt1(j,1)
      z2t=pt2(j,2)-pt1(j,2)

      xl=xt*cos(th(j))+zt*sin(th(j))
      zl=-xt*sin(th(j))+zt*cos(th(j))
      x2l=x2t*cos(th(j))+z2t*sin(th(j))
      z2l=0.

        if(xl.gt.0..and.xl.lt.abs(pt1(j,1)-pt2(j,1)).and.
     &  zl.gt.0..and.zl.lt.core*.2) then
         i1=j
         end if

      r1=sqrt(xl**2+zl**2)
      r2=sqrt( (xl-x2l)**2+zl**2 )
      th1=atan2(zl,xl)
      th2=atan2(zl,xl-x2l)

      uls= 1./(2.*pi)*log(r1/r2)
        ulv= 1./(2.*pi)*(th2-th1)
      wls= 1./(2.*pi)*(th2-th1)
```

```fortran
      wlv= 1./(2.*pi)*log(r2/r1)

      uwing = uwing +  (uls*g(j) + ulv*g(m+1) )*cos(-th(j))
     & +( wls*g(j) + wlv*g(m+1) )*sin(-th(j))
      wwing = wwing + (-uls*g(j) - ulv*g(m+1) )*sin(-th(j))
     & +( wls*g(j) + wlv*g(m+1) )*cos(-th(j))

      end do
      else
      end if

c     freestream influence
      uinf = 0.
      winf = 0.
      if(i2.eq.1)then

      uinf = cos(alpha)
      winf = sin(alpha)
      else
      end if

c     vortex influence

      uvort = 0.
      wvort = 0.

      if(i4.eq.0)then
        istrt = itime - 1
      else
        istrt = itime
      end if

      do j=istrt,1,-1

         do i=1,nsep

         xv = vposo(i,1,j)*cos(alpha) - vposo(i,2,j)*sin(alpha)
         zv = vposo(i,2,j)*cos(alpha) + vposo(i,1,j)*sin(alpha)+h
         r=sqrt((x-xv)**2+(z-zv)**2)

        if(r.gt.0.0000001)then
       uvt=gam(i,j)/(2.*pi)*( (z-zv)/r**2 )
     &    * ( 1. - exp(-1.256*(r/core)**2) )
       wvt=-gam(i,j)/(2.*pi)*( (x-xv)/r**2 )
     &    * ( 1. - exp(-1.256*(r/core)**2) )
        else
        end if

      uvort = uvort + uvt
      wvort = wvort + wvt

        end do
      end do

       u = uwing + uinf + uvort
       w = wwing + winf + wvort
      return
      end
```

```
'*****************************************************************
'           program           sim.bas                          *
'           written by:       Todd Perfito                     *
'           May, 1994         Oklahoma State University        *
'                                                              *
'      This program animates the flowfield from the output    *
'      generated by the program wingsep.  It also shows the   *
'      vorticity strengthm of the shed vortices by scaling    *
'      the color of each vortex relative to the minimum       *
'      and maximum vortex strengths.                          *
'                                                              *
'*****************************************************************
open "c:anm1.dat" for input as #1
open "c:afoil40.dat" for input as #2
input #1, istepm, delt, nskip, xcg
skip = 1
q = 1
istepm = 100

dim vloc(istepm, istepm, 2), v2loc(istepm, istepm, 2), wing(41, 2)

dim al(istepm + 1), h(istepm + 1), gam(2, istepm)

dim pal&(20)

print " enter scale factor": input sx

2 sz = sx * 1.1
ar = 1
if q = 2 then goto 3

'         BLUES
index = 1
blue = 63
for i = 0 to 54 step 9
 red = i
 green = i
 pal&(index) = 65536 * blue + 256 * green + red
 index = index + 1
next i

'         REDS
index = 8
red = 63
for i = 44 to 0 step -10
blue = i
green = i
pal&(index) = 65536 * blue + 256 * green + red
index = index + 1
next i

'         GREEN, BLACK, & WHITE
pal&(13) = 65536 * 0 + 256 * 40 + 0
pal&(7) = 65536 * 63 + 256 * 63 + 63
pal&(0) = 0
pal&(15) = 65536 * 63 + 256 * 63 + 63


3 x = delt * istepm * nskip
```

76

```
z = delt * istepm * nskip
zz = z
xx = x
screen 12
palette using pal&
window (-1, z * sz + 1)-(x * sx + 1, -z * sz)
if q = 2 then goto 1

locate 22, 1
print "loading..."

for i = 1 to istepm
 input #1, t, al(i), h(i)

   for j = 1 to i
     input #1, x, z, gamma
     vloc(i, j, 1) = x
     vloc(i, j, 2) = z
     gam(1, i) = gamma
     if i = 1 then gammin = gamma
   next j

   for k = 1 to i
     input #1, x, z, gamma
     v2loc(i, k, 1) = x
     v2loc(i, k, 2) = z
     gam(2, i) = gamma
     if i = 1 then gammax = gamma
   next k

next i




if abs(gammin) > gammax then gamsprd = abs(2 * gammin)
else gamsprd = 2 * gammax gammax = gamsprd / 2
gammin = -gammax

for i = 1 to 41
 input #2, x, z
 wing(i, 1) = x - xcg
 wing(i, 2) = z
next i
al(0) = al(1)

1 cls

for i = 2 to 12
 r = delt * i * zz / 1.1
line (-1, 1 + sz * (zz - r - 1.5))-(-1 + (xx * sx + 1) * .04,
   1 + sz * (zz - r + delt * 12 - 1.5)), i, bf
next i

locate 3, 4
print using "###.##"; gammin
locate 6, 4
print using "###.##"; 0!
locate 9, 4
print using "###.##"; gammax
```

```
locate 2, 15
print "time"
locate 2, 25
print "alpha"

for i = 1 to istepm
 circle (0, 0), .01, 4
 if i mod skip = 0 then
 locate 3, 13
 print using "###.##"; i * delt * nskip
 locate 3, 24
 print using "###.##"; al(i) * 180 / 3.14159

 for k = 1 to 40
  x = wing(k, 1) * cos(al(i - skip)) + wing(k, 2) * sin(al(i - skip))
  z = -wing(k, 1) * sin(al(i - skip)) + wing(k, 2) * cos(al(i - skip))-
h(i - skip)
  x1 = wing(k + 1, 1) * cos(al(i - skip)) + wing(k + 1, 2) * sin(al(i -
skip))
  z1 = -wing(k + 1, 1) * sin(al(i - skip)) + wing(k + 1, 2) * cos(al(i
- skip))- h(i - skip)
  line (x, z)-(x1, z1), 0
  x = wing(k, 1) * cos(al(i)) + wing(k, 2) * sin(al(i))
  z = -wing(k, 1) * sin(al(i)) + wing(k, 2) * cos(al(i)) - h(i)
  x1 = wing(k + 1, 1) * cos(al(i)) + wing(k + 1, 2) * sin(al(i))
  z1 = -wing(k + 1, 1) * sin(al(i)) + wing(k + 1, 2) * cos(al(i)) -
h(i)
  line (x, z)-(x1, z1), 13
 next k

 for j = 1 to i
  temp = abs(int((gam(1, j) - gammin) / gamsprd * 11))
  if temp = 0 then temp = 1
  circle (vloc(i - skip, j, 1), vloc(i - skip, j, 2)), .01, 0
  circle (vloc(i, j, 1), vloc(i, j, 2)), .01, temp
  temp = abs(int((gam(2, j) - gammin) / gamsprd * 11))
  circle (v2loc(i - skip, j, 1), v2loc(i - skip, j, 2)), .01, 0
  circle (v2loc(i, j, 1), v2loc(i, j, 2)), .01, temp
 next j

 rem for l = 1 to 50000 * exp(-i / 25)
 rem next l
 end if
 a$ = inkey$
 if a$ = chr$(27) then stop
 if i = istepm then 100
next i

100 locate 27, 74
print "go again? (1-y,0-n, or 2-scaling)" locate 3, 48: input q
if q = 1 then
 goto 1
elseif q = 2 then
 goto 1000
end if
goto 1001

1000 locate 27, 74: print "enter scale factor" locate 3, 48: input sx:
goto 2
```

```
1001 close #1
end
```

γ

VITA

Todd Kirkland Perfito

Candidate for the Degree of

Master of Science

Thesis: A 2D UNSTEADY INVISCID MODEL OF SEPARATED FLOW PAST
            AN AIRFOIL

Major Field: Mechanical Engineering

Biographical:

   Personal Data: Born in San Antonio, Texas, on August 7, 1965, the son of Joseph
       C.and Patricia D. Perfito

   Education: Graduated from Jenks High School, Tulsa, Oklahoma in May, 1983:
       received Bachelor of Science degree in Mechanical Engineering from
       Oklahoma State University, Stillwater, Oklahoma in May, 1992. Completed
       the requirements for the Master of Science degree with a major in Mechanical
       Engineering at Oklahoma State University in December, 1994.

   Experience: Enlisted in the United States Air Force in 1984 as an aircraft
       mechanic,(crew chief), on the Lockheed C-130 until 1988; employed as a
       flight line technician at the local airport in Stillwater, Oklahoma as an
       undergraduate; employed by Oklahoma State University, Department of
       Mechanical and Aerospace Engineering as an undergraduate teaching
       assistant and as a graduate research assistant until July, 1994; presently
       employed at Boeing Commercial Airplane Group in Wichita, Kansas as a
       Manufacturing Research & Development Engineer.

   Professional Membership: American Institute of Aeronautics and Astronautics.